

**Anisotropic Hydraulic Conductivity of Faulted
Poorly Consolidated Eolian Sands: Bosque, New Mexico**

by

Sung-ho Hong


Submitted in partial fulfillment
of the requirements for the degree of
Master of Science of Geology

New Mexico Institute of Mining and Technology
Department of Earth and Environmental Science
Socorro, New Mexico

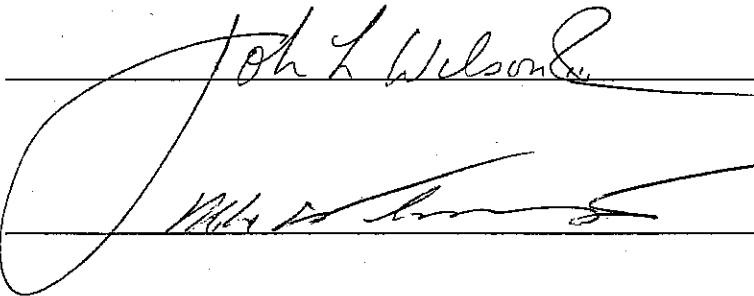
January, 1999

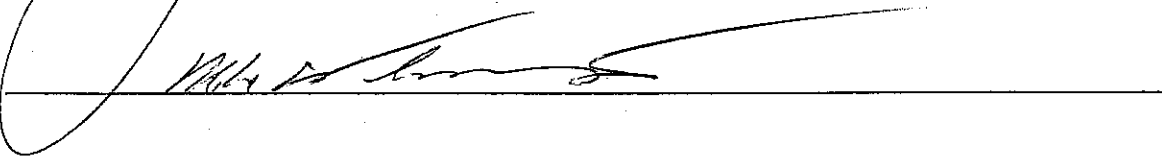
APPROVAL

This thesis is accepted on behalf of the faculty
of the Institute by the following committee.



Adviser

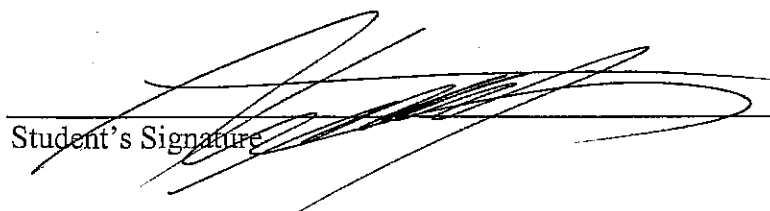




1/15/99

Date

I release this document to New Mexico Institute of Mining and Technology.



Student's Signature

01/14/99

Date

ACKNOWLEDGEMENTS

I would like to thank to my wife Youn-A, and my parents for their support and putting up with me during my master's program.

I would like to express my sincere gratitude to Dr. Mike Whitworth for his guidance, advice, and helpful discussions during both the research and writing phases of this project, and also thank the rest of my committee members, Drs. Peter Mozley and John Wilson for their advice and encouragement regarding my research.

I also wish to acknowledge Dr. Laurel Goodwin, and graduate students, John Sigda, Matt Herrin, Jeff Rawling, and Ron Smith. All of you helped out in ways that made my research more bearable and productive.

ABSTRACT

Small-scale faults (< 1 m displacement) in poorly consolidated sediments produce low hydraulic conductivity deformation bands ranging from much less than one centimeter to several centimeters in thickness. The purpose of this study is to measure the hydraulic conductivity of deformation bands as well as the three-dimensional hydraulic conductivity of the poorly consolidated surrounding matrix sands in order to investigate the likelihood that these small displacement faults might significantly influence fluid and chemical movement.

The study area is located about 20 miles south of Socorro, New Mexico within the Bosque del Apache National Wildlife Refuge in the Socorro Basin. At the study site, the faulted lower Santa Fe Group (middle Miocene to late Oligocene) eolian facies are characterized by poorly consolidated and well- to moderately-sorted fine- to coarse-grained sands, and large-scale cross-stratification and planar bedding. Deformation bands are abundant in the study area and exhibit smaller grain size, poorer sorting, and lower hydraulic conductivity than the surrounding undeformed sediments

Oriented, undisturbed samples from both undeformed and deformed sediments were collected in the field, and hydraulic conductivities were measured in the laboratory using a flexible-wall permeameter. The hydraulic conductivity of undeformed sediments parallel to bedding ranged from 2.29×10^{-3} to 1.63×10^{-2} cm/s, and perpendicular to bedding ranged from 2.11×10^{-3} to 6.65×10^{-3} cm/s. The mean ratio of hydraulic conductivity between parallel and perpendicular to bedding was 1.43. Hydraulic conductivities parallel to dip were 4 to 20% higher than those parallel to strike, however, the precision of the measurements was not sufficient to say that this difference is

significant. Hydraulic conductivity perpendicular to deformation bands is four orders of magnitude less than the undeformed host sediments and ranges from 2.52×10^{-7} to 3.93×10^{-7} cm/s.

The major cause of anisotropy in the undeformed sediments is probably depositional controls on grain orientation and bedding structure. Hydraulic conductivity reduction in individual deformation bands may have been caused by cataclasis, rotation of grain fragments, increased clay content, and diagenetic alteration. The results of the hydraulic conductivity measurements support the concept that depositional and deformational processes may influence hydraulic conductivity and its anisotropy in faulted poorly consolidated sediments.

TABLE OF CONTENTS

	Page
LIST OF FIGURES.....	vii
LIST OF TABLES.....	ix
INTRODUCTION.....	1
GEOLOGY.....	5
METHODS.....	10
RESULTS.....	23
DISCUSSION.....	37
SUMMARY AND CONCLUSIONS.....	43
RECOMMENDATIONS FOR FUTURE WORK.....	45
REFERENCES.....	46
APPENDIX.....	50

LIST OF FIGURES

	Page
FIGURE 1: Rio Grande rift basins of New Mexico.....	6
FIGURE 2: Location map of the study area.....	8
FIGURE 3: Orientation of hydraulic conductivity measurements in deformed sands.....	11
FIGURE 4: Orientation of sampling in undeformed sands.....	13
FIGURE 5: Schematic of flexible wall permeameter.....	14
FIGURE 6: Plot of head loss versus flow rate Q for empty permeameter with stainless steel screens.....	17
FIGURE 7: Plot of head loss versus flow rate Q for empty permeameter with porous stones.....	19
FIGURE 8: Lithology and structure of Site 1.....	24
FIGURE 9: Lithology and structure of Site 2.....	26
FIGURE 10: Location and distribution of hydraulic conductivity (cm/s) at Site 1.....	28
FIGURE 11: Location and distribution of hydraulic conductivity (cm/s) at Site 2.....	30
FIGURE 12: Plot of hydraulic conductivity of all samples.....	33
FIGURE 13: Plot demonstrating the decrease of flow rate Q over time (undeformed sand, perpendicular to bedding, Site 1a).....	34
FIGURE A1: Hydraulic conductivity of undeformed sands, Site 1.....	65
FIGURE A2: Hydraulic conductivity of undeformed sands, Site 2.....	66
FIGURE A3: Hydraulic conductivity of perpendicular to deformation bands; homogeneous sample, Site 1 and 2.....	67
FIGURE A4: Hydraulic conductivity of deformation zone; parallel to deformation bands in composite sample, Site 1 and 2.....	68
FIGURE A5: Hydraulic conductivity of deformation zone; perpendicular to deformation bands in composite sample, Site 1 and 2.....	69

FIGURE A6: Variation of hydraulic conductivity of perpendicular to deformation bands70

LIST OF TABLES

	Page
TABLE 1: Hydraulic conductivity of undeformed sands.....	29
TABLE 2: Hydraulic conductivity of deformed sands.....	31
TABLE 3: Hydraulic conductivity versus thickness of deformation bands in homogeneous samples.....	31
TABLE 4: X-ray diffraction sample description.....	35
TABLE 5: Mineralogy of clay-size fraction.....	36
TABLE 6: Particle size analysis.....	36
TABLE A1: Site 1a, hydraulic conductivity and permeability data for undeformed sand; perpendicular to bedding.....	52
TABLE A2: Site 1a, hydraulic conductivity and permeability data for undeformed sand; parallel to strike.....	52
TABLE A3: Site 1a, hydraulic conductivity and permeability data for undeformed sand; parallel to dip direction.....	52
TABLE A4: Site 1b, hydraulic conductivity and permeability data for undeformed sand; perpendicular to bedding	53
TABLE A5: Site 1b, hydraulic conductivity and permeability data for undeformed sand; parallel to strike.....	53
TABLE A6: Site 1b, hydraulic conductivity and permeability data for undeformed sand; parallel to dip direction.....	53
TABLE A7: Site 2a, hydraulic conductivity and permeability data for undeformed sand; perpendicular to bedding.....	54
TABLE A8: Site 2a, hydraulic conductivity and permeability data for undeformed sand; parallel to bedding, XX orientation.....	54
TABLE A9: Site 2a, hydraulic conductivity and permeability data for undeformed sand; parallel to bedding, YY orientation.....	54
TABLE A10: Site 2b, hydraulic conductivity and permeability data for undeformed sand; perpendicular to bedding.....	55

TABLE A11: Site 2b, hydraulic conductivity and permeability data for undeformed sand; parallel to bedding, XX orientation.....	55
TABLE A12: Site 2b, hydraulic conductivity and permeability data for undeformed sand; parallel to bedding, YY orientation.....	55
TABLE A13: Site 1, hydraulic conductivity and permeability data for undeformed sand; upper fine layer, parallel to bedding.....	56
TABLE A14: Site 1, hydraulic conductivity and permeability data for undeformed sand; intercalated coarse lens, parallel to bedding.....	56
TABLE B1: Site 1, hydraulic conductivity and permeability data for deformation band; perpendicular to deformation band; sample A.....	56
TABLE B2: Site 1, hydraulic conductivity and permeability data for deformation band; perpendicular to deformation band; sample B.....	57
TABLE B3: Site 2, hydraulic conductivity and permeability data for deformation band; perpendicular to deformation band; sample A.	57
TABLE B4: Site 2, hydraulic conductivity and permeability data for deformation band; perpendicular to deformation band; sample B.	58
TABLE C1: Site 1, hydraulic conductivity and permeability data for deformation zone; parallel to deformation bands (0.3cm) and normal to bedding; sample C.....	58
TABLE C2: Site 1, hydraulic conductivity and permeability data for deformation zone; parallel to deformation bands (1.5cm) and parallel to bedding; sample D.....	59
TABLE C3: Site 2, hydraulic conductivity and permeability data for deformation zone; parallel to deformation bands (0.4cm) and parallel to bedding; sample C.....	59
TABLE C4: Site 2, hydraulic conductivity and permeability data for deformation zone parallel to deformation bands (0.2cm) and parallel to bedding; sample D.....	60
TABLE C5: Site 1, hydraulic conductivity and permeability data for deformation zone; perpendicular to deformation bands (0.2cm) and parallel to bedding; sample E.....	60

TABLE C6: Site 1, hydraulic conductivity and permeability data for deformation zone; perpendicular to deformation bands (0.6cm) and parallel to bedding; sample F.....	61
TABLE C7: Site 1, hydraulic conductivity and permeability data for deformation zone; perpendicular to deformation bands (1.4cm) and parallel to bedding; sample G.....	61
TABLE C8: Site 1, hydraulic conductivity and permeability data for deformation zone; perpendicular to deformation bands (1.5cm) and parallel to bedding; sample H.....	62
TABLE C9: Site 2, hydraulic conductivity and permeability data for deformation zone; perpendicular to deformation bands (0.1cm) and parallel to bedding; sample E.....	62
TABLE C10: Site 2, hydraulic conductivity and permeability data for deformation zone; perpendicular to deformation bands (0.3cm) and parallel to bedding; sample F.....	63
TABLE C11: Site 2, hydraulic conductivity and permeability data for deformation zone; perpendicular to deformation bands (0.2cm) and parallel to bedding; sample G.....	63
TABLE C12: Site 2, hydraulic conductivity and permeability data for deformation zone; perpendicular to deformation bands (0.5cm) and parallel to bedding; sample H.....	64

INTRODUCTION

The influence of faults on fluid flow is not well understood. However some models of fluid flow in faults at various scales have been proposed (e.g. Davis and DeWeist, 1966; Huntoon and Lundy, 1979; Maclay and Small, 1983; Haneberg, 1994). Faults may act as either conduits or barriers to fluid flow (Knipe, 1993; Knipe and McCaig, 1994; Cox, 1994; Gibson, 1994).

It is important to understand the role that faults play in the movement of water and chemicals in the subsurface. Faults can have an impact on water supply, petroleum migration and trapping, diagenesis, and movement or immobilization of contaminant plumes. Near-surface small-scale (less than one-meter of displacement) faults in poorly consolidated materials are especially important because they may impact 1) water supply, 2) movement of dissolved contaminants, and/or 3) movement of free-phase non aqueous phase liquids such as gasoline or chlorinated hydrocarbons.

Most of the work on small displacement faults in sedimentary deposits has focused on well-consolidated sandstone and these small displacement faults exhibit an order of magnitude porosity decrease and have hydraulic conductivities three orders of magnitude less than the surrounding parent rock (Aydin and Johnson, 1983; Antonellini and Aydin, 1994). Although small displacement faults are common in poorly consolidated sediments, such as the Santa Fe Group sediments in the Rio Grande rift, they are too small to be included on geologic maps and very little is known about their hydrologic characteristics and spatial distribution. Sigda (1997) measured fault zone hydraulic conductivities for small displacement faults in poorly consolidated sediments using in-situ air permeametry and showed that hydraulic conductivities of the deformed

sediments are two to three orders of magnitude less than that of the undeformed sediments.

Deformation bands, narrow zone of cataclasis, are mostly associated with small displacement faults, and they have displacements of a few mm to tens of cm and thicknesses as low as 1mm. Deformation bands and deformation zones (cataclastic slip zone, i.e., zones of closely spaced deformation bands) typically have a lighter color and a higher resistance to weathering, even though they have essentially the same mineralogical and chemical compositions as the surrounding parent sandstone (Antonellini and Aydin, 1994). Mozley and Goodwin (1995) studied deformation bands in poorly consolidated Santa Fe Group sediments and found that they are characterized by grain fracturing and/or elongate grain orientation within several centimeters of a given deformation band boundary. They also mentioned that some small displacement faults that exhibit little to no deformation were also preserved within the fault zone. If deformation bands in poorly or unconsolidated sands have low conductivities like those in well-consolidated sediments, as suggested by Sigda (1997), they may act as natural barriers to single phase fluid flow, and may subdivide aquifers into compartments, thereby affecting the movement of water and hydrocarbons and possibly influencing diagenesis (Smith, 1980; Pittman, 1981; Bevan, 1985; Nelson, 1985; Hardmann and Booth, 1991; Antonellini and Aydin, 1994).

Several previous studies deal with conductivity anisotropy in undeformed sediments. The first mention of conductivity anisotropy in sandstone might be Newell (cited in King, 1899) who noticed in 1885 that in natural sandstone, hydraulic conductivity was greater parallel to bedding than perpendicular to it. Hutta (1956)

studied the relationship between fabric orientation of sands and hydraulic conductivity variation in the plane of bedding with 35 samples from varied rock types, and he mentioned that there is no significant correlation between fabric orientation of sands and hydraulic conductivity variation in the plane of bedding. Griffiths (1961) documented that the quartz grain orientation from Bardford sand was found to lie at an angle with respect to bedding, so that the maximum hydraulic conductivity may be parallel to the angle of inclination of the grains rather than parallel to bedding. Mast and Potter (1963) measured imbibition rate in late Mississippian and Pennsylvanian sandstones of the Illinois Basin and found that maximum imbibition direction was parallel not only to the maximum hydraulic conductivity direction but also the mean fabric orientation. Fondeur (1964) estimated anisotropy in the silicified Hassi Messaoud Sandstone (Cambrian) of Algeria, and found vertical hydraulic conductivity to be 25 to 50% less than horizontal hydraulic conductivity, but found little hydraulic conductivity difference in the horizontal direction. Greenkorn et al. (1964) measured the hydraulic conductivity of 142 sandstone samples using an air permeameter and noted that in sandstone hydraulic conductivity was approximately 30% lower perpendicular to bedding than parallel to it. Greenkorn et al. (1964) did not discuss the depositional environments of the sandstones he studied. Using borehole dilution tests and permeameter measurements at Twin Lakes, Killey and Motyaner (1988) estimated the ratio of horizontal to vertical hydraulic conductivity as 1.1 to 10.8 in a fluvial sand aquifer. Most recently, Burger and Belitz (1997) measured hydraulic conductivity of unconsolidated sands in a Holocene shoreface deposit for sixty-four samples using a constant head permeameter and found that the ratio of horizontal to vertical hydraulic conductivity ranged from 1.33 to 1.57.

The purpose of this study was to measure the hydraulic conductivity anisotropy of both deformation bands and undeformed sands in a relatively unconsolidated sand so that the effect of the lower hydraulic conductivity deformation zones associated with small faults on fluid movement and chemical transport might be deduced. A flexible-wall permeameter was chosen for this study because 1) unlike in-situ air permeametry, directional hydraulic conductivities can easily be measured, and 2) the local groundwater could be used so pore throat clogging from clay swelling would be comparable to what would be expected in the water saturated subsurface.

Hydraulic conductivity measurements are strongly scale-dependent (Neuman, 1990) and interpretations derived from bedding-scale measurements, such those in this study, are not likely to be definitive at significantly larger scales. However, it is important to begin to characterize hydraulic conductivity variations and differences between and within the poorly consolidated sand matrix and the deformation zones created by small, sub-meter-scale faults, because these small features are currently ignored in water resources planning and site-scale contaminant transport modeling.

GEOLOGY

The study area is located in the southern part of the Socorro Basin (Fig. 1) and lies within the lower Santa Fe Group. The Rio Grande rift separates the Colorado Plateau to the west from the interior of the craton to the east (Chapin and Cather, 1994). Approximately 30 million years ago the extensional processes that characterize continental rifting began. Large crustal segments tilted and sank relative to adjacent elevated mountain blocks and created thick basin fill deposits, ultimately resulting in the formation of the Rio Grande rift basins, including the Albuquerque and Socorro Basins (Kelley, 1977; Cather, 1992).

The Santa Fe Group is divided into lower, middle, and upper units (Hawley et al., 1995). The sediments of the lower Santa Fe Group range from approximately 25 to 15 million years age (Hawley et al., 1995). The Santa Fe Group consists of interbedded, fine-grained sand and clay, which is indicative of a low to moderate energy environment (Lozinsky and Tedford, 1991). With regard to Socorro Basin, the Popatosa Basin, an ancestor to the modern-day basins, extended about 50% during the Oligocene and Miocene (Chapin and Cather, 1994). During the Miocene, the Popatosa Basin separated into the La Jencia and Socorro Basins with the uplift of the Lemitar-Socorro Mountains (Cather et al., 1994). The Socorro Basin is composed of an unknown thickness of alluvial fill, probably up to several thousand feet, and is bounded by outcrops of Paleozoic rocks to the east and Tertiary volcanic, Paleozoic, and Precambrian rocks to the west (Anderholm, 1983). The primary aquifer of the Socorro Basin contains Tertiary and Quaternary alluvial fill deposits. The upper units of the alluvial deposit mainly consist of

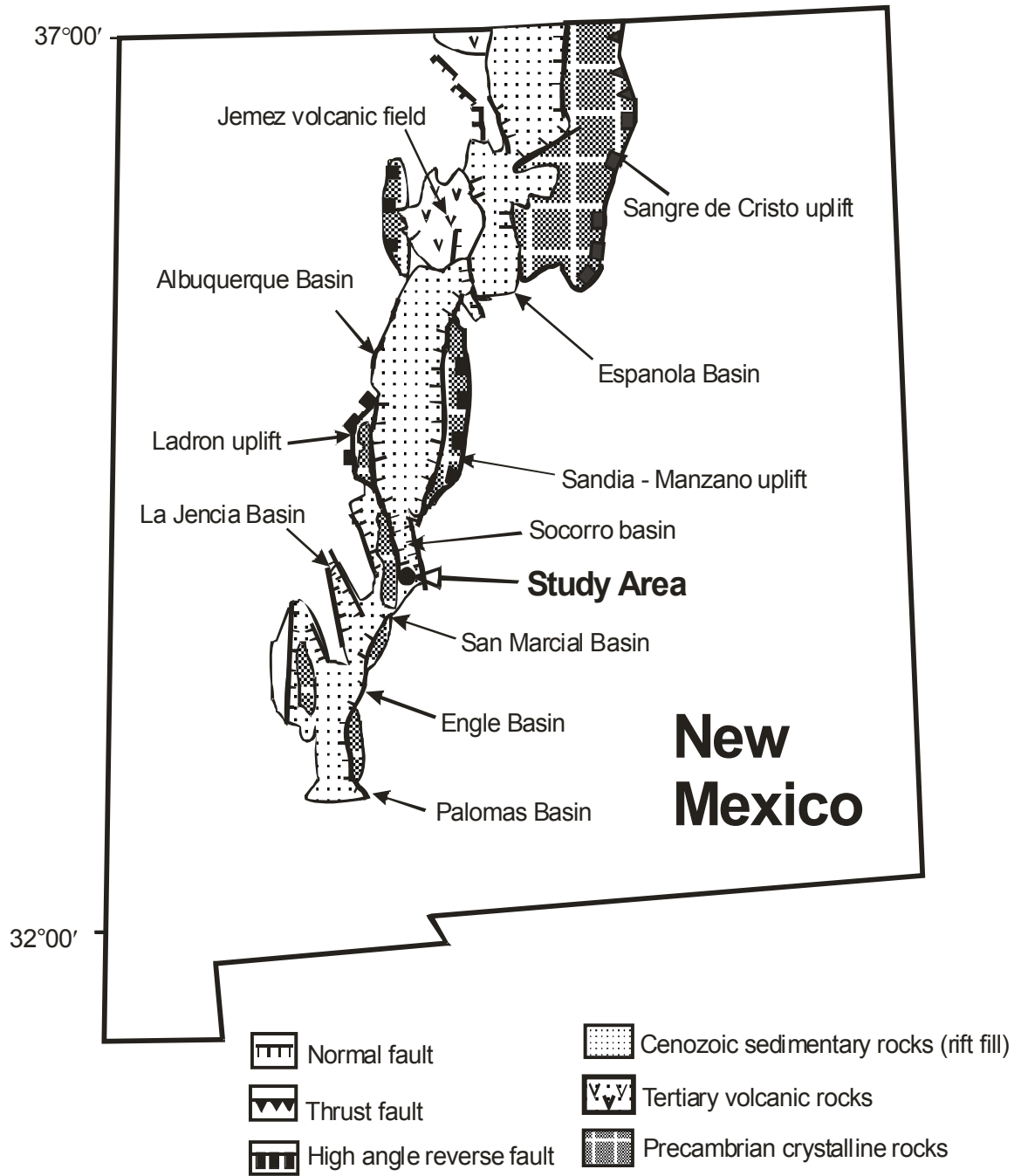


Figure 1. Rio Grande rift basins of New Mexico (after Russel and Snelson, 1994).

sand and gravel, with some clay layers. These deposits are relatively conductive; however, deeper strata may consist of less conductive indurated clays and evaporites (Anderholm, 1983).

The study area is located about 20 miles south of Socorro, New Mexico (Fig. 2). The study area lies along the east side of a railroad cut that is adjacent to the Canyon Trail in the Bosque del Apache Wildlife Refuge approximately 1.4 miles south of the Visitor's Center on the west side of NM Route 1. The sampling sites are located 20 m apart along the same railroad cut. In this area, numerous faults with displacements ranging from a few millimeters to tens of centimeters cut poorly consolidated lower Santa Fe Group sediments of middle Miocene to late Oligocene age (Davis, 1994). The sediments in the railroad cut consist of eolian, fluvial, and alluvial fan facies. The eolian facies in the study area is about 1.5 m thick and is characterized by poorly consolidated and well to moderately sorted silty fine- to coarse-grained sand, and exhibits large scale tangential cross-stratification and planar bedding. This study was conducted entirely within the eolian facies. The deformation bands are lighter in color and better indurated than the surrounding undeformed sands when the outcrop is dry. However, when the outcrop is damp, it is difficult to distinguish individual deformation bands from the surrounding sand matrix by differences in color and hardness. This suggests that the bands are clay-mineral rich.

The faults are small normal faults. They typically dip 60° to 80° in a southerly direction. A few dip to the north. The width of the deformed zones varies from a few mm to tens of mm. Fault zones tend to be wider towards the base of the outcrop. Foliation or lineation is subparallel to slip direction in the vicinity, but was not

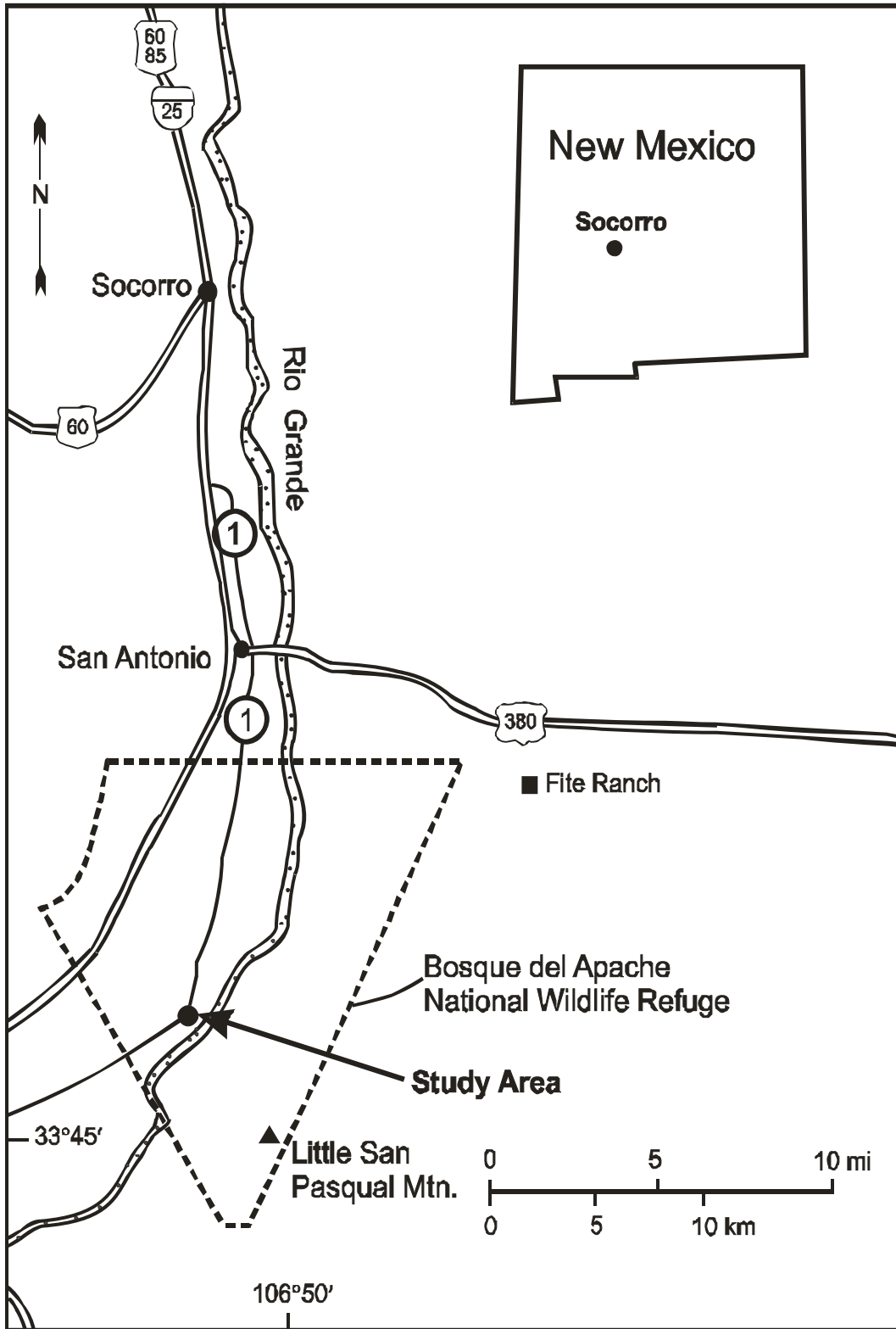


Figure 2. Location map of the study area (after Geddes, 1993).

observable at the study sites, therefore, the total vertical displacement of individual deformation bands and fault zones was estimated by marker bed or contact displacement.

METHODS

First, two sites were selected that exhibited a relatively simple distribution of undeformed and deformed zones. Next, samples were collected in the field. When the outcrop was relatively dry, sampling was performed using a 1⁵/₈-inch diameter hole saw with center drill removed. When the outcrop was damp, the sand was too friable for sampling with a hole saw, so orientation markings were applied to the surface of the outcrop and cubes of sediment approximately 30 cm on each side were collected. The blocks were then oven-dried at 105°C and sampled using a 1⁵/₈-inch hole saw. After a core was removed from the hole saw, it was shaped by carefully rubbing the sample between two wooden blocks containing 1.5-inch radius grooves to reduce the diameter to 1.5-inches.

Preparing a deformation band sample required exceptional care because the bands are generally less than 1 cm thick and are easily broken. The smallest deformation bands, less than 1 mm thick, could not be separated from the undeformed sands. For these thin deformation bands, samples were prepared which also contained undeformed sands and the hydraulic conductivity of the deformation band was estimated using an inverse harmonic or arithmetic mean model, as appropriate for the sample orientation. Figure 3 shows how hydraulic conductivity was measured in relation to the deformation bands in composite sample.

Sixteen samples were collected from Site 1. Of these, eight consisted of undeformed sands and eight contained one or more deformation bands. Cores from the undeformed sands were obtained with three orientations: 1) parallel with bedding and parallel with strike, 2) parallel to bedding and parallel to dip, and 3) perpendicular to

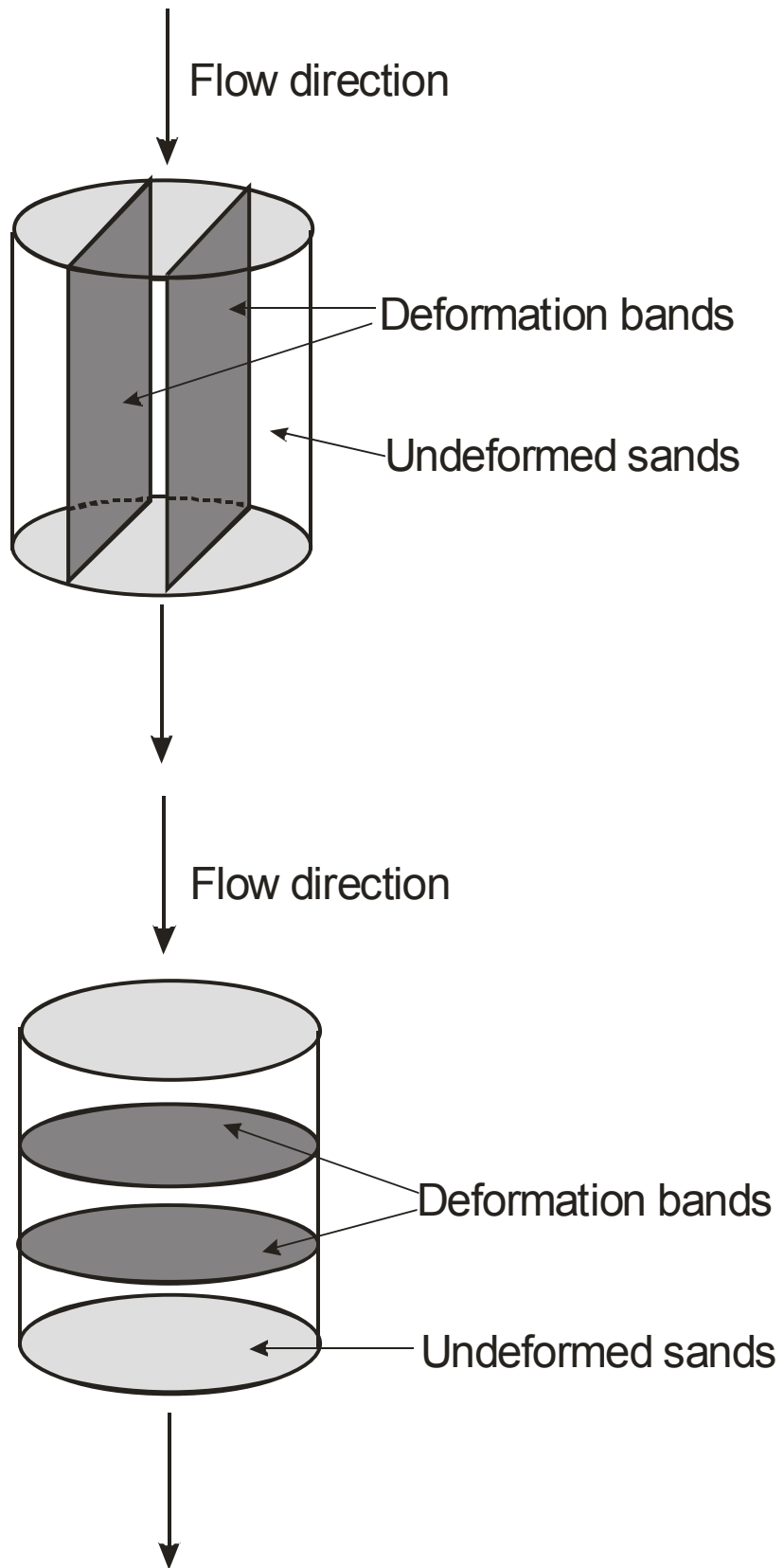


Figure 3. Orientation of hydraulic conductivity measurements in deformed sands.

Figure 4 delineates the orientation of the undeformed samples. Of the samples containing deformation bands, two consisted of only deformation bands (thickness: 0.6 and 0.3 cm) with all sand removed, and six consisted of thin deformation bands sandwiched within matrix sand. Of the six samples of deformation bands sandwiched in matrix sand, four were oriented perpendicular to the deformation bands and two were oriented parallel to the deformation bands.

Fourteen samples were collected from Site 2. Six were collected from undeformed sands, two each parallel with bedding and parallel with the outcrop, parallel to bedding and perpendicular to the outcrop, and perpendicular to bedding. Eight samples were collected containing deformed material. Of these, two consisted of only deformation band material (thickness: 0.3 and 0.2 cm), four were oriented perpendicular to the deformation bands and sandwiched in matrix sand, and two were oriented parallel to the deformation bands and sandwiched in matrix sand.

After preparation, the length of each sample core was measured and it was placed into the flexible-wall permeameter (Fig. 5). The 1.5-inch diameter core was confined by a rubber membrane, which was subjected to an external hydrostatic pressure in excess of the head applied to the sample during hydraulic conductivity measurement. The rubber membrane ensures there is no leakage along the sides of the specimen. The procedure for using the flexible wall permeameter is as follows:

1. Prepare a 1.5-inch diameter core specimen. Measure and record the length and cross-sectional area of the specimen.
2. De-air the water in both the supply reservoir and the constant head reservoir by placing it under vacuum. This usually takes about one hour. For this procedure

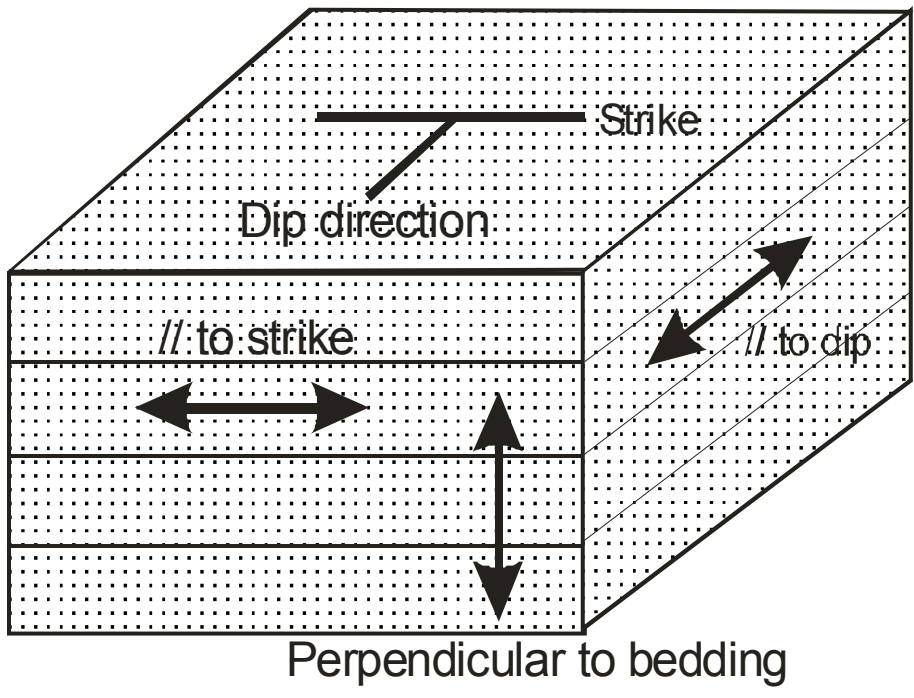


Figure 4. Orientation of sampling in undeformed sands.

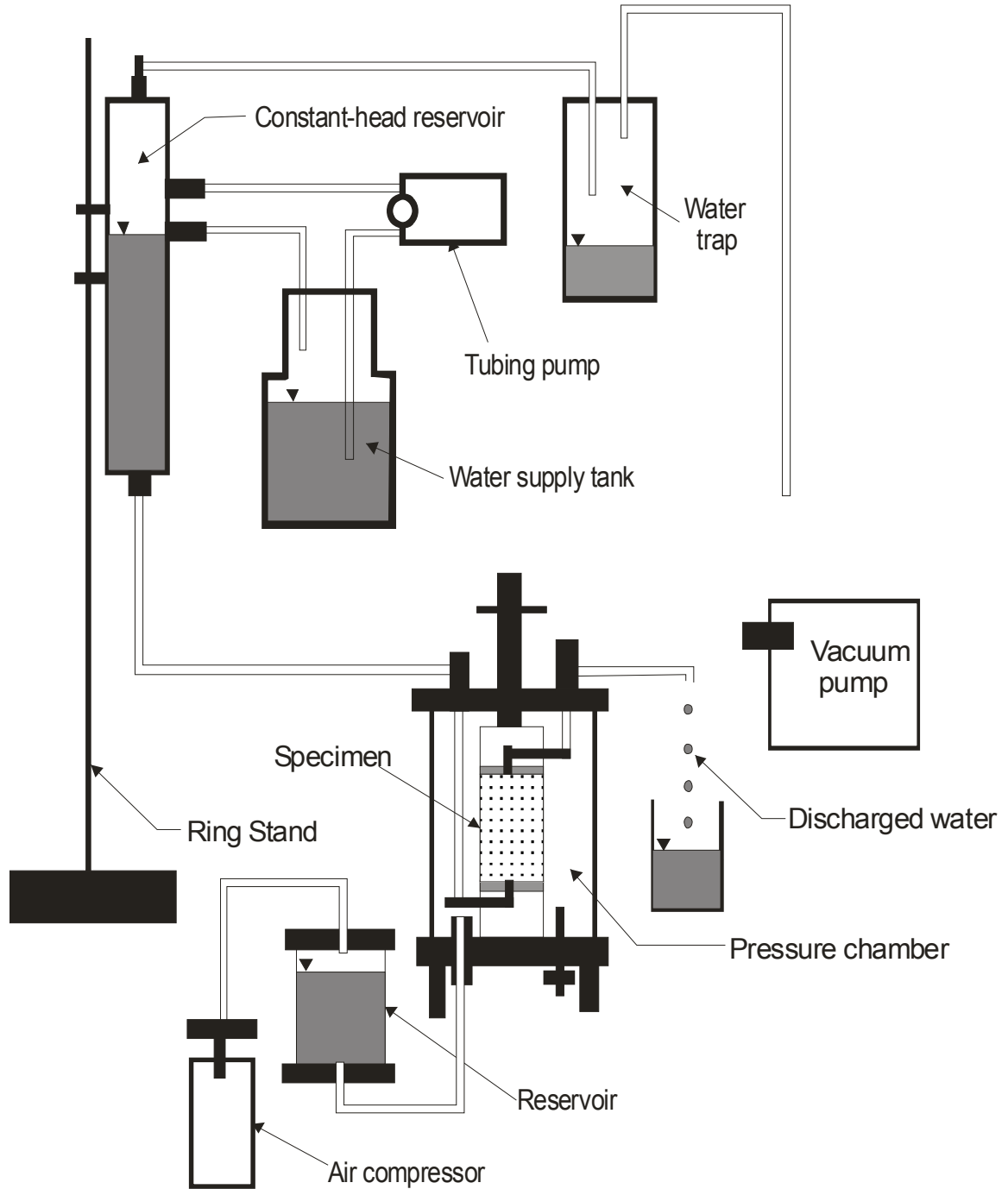


Figure 5. Schematic of flexible wall permeameter.

the constant head reservoir is connected to the water supply reservoir and both are connected to the vacuum pump.

3. Load the specimen in the permeameter with either 316 stainless steel screens (for undeformed sand samples) or porous stones (for deformation band samples) placed at each end of the core. Porous stones were used because they provide greater support for the fragile deformation band samples. The water outlet tube is then connected to the vacuum pump, the valve between the constant-head reservoir and permeameter is closed, and the core is placed under vacuum for approximately one hour while constrained by the rubber membrane.
4. The chamber surrounding the flexible liner is then filled with water and pressurized using lab air. When a head difference of 10 cm was used across the sample, the chamber pressure was set at 10 psi, which is equivalent to 704 cm of head. The chamber pressure should not be less than the maximum head on the sample during the test.
5. The valve between the vacuum pump and the permeameter outlet is then closed, so that the sample remains under vacuum, and the water inlet valve is opened and the sample is allowed to saturate with de-aired water. The outlet valve is not opened until the sample is fully saturated.
6. The volume of water discharging is then periodically recorded. To maximize accuracy, the volume of each aliquot is determined gravimetrically to two decimal places. Measurements continue until steady state is reached and the flow is no longer changing over time. Steady state is defined as when there is no change in flow rate for three consecutive measurements over a time period of at least one hour. For

samples with very low hydraulic conductivity, such as the deformation bands, the volume of water discharging at an applied head of 10 cm was quite small and difficult to measure accurately. Therefore, for these samples, a syringe pump (ISCO Model 500D) was used to provide a constant head of up to 2,886 cm (41 psi). A correspondingly greater fluid pressure was used in the outer chamber as necessary. The major procedural difference was that de-aired water was loaded into the 500 ml capacity syringe pump, and then fed directly into the flexible wall permeameter after the sample was placed under a vacuum. Each of these samples was run to steady state.

Calculation Methods

Hydraulic conductivities K were calculated from

$$K = \frac{VL}{Ath} \quad (1)$$

where V is the volume of water collected in cm^3 , L is the length of the sample in cm, A is the area of the sample in cm^2 , t is time in seconds, and h is head difference in centimeters. To effectively use Equation 1, the value h must first be corrected for the permeameter head loss (Burger and Belitz, 1997). This is done by first measuring the flow rate Q in $\text{cm}^3/\text{minute}$ through the empty permeameter for differing heads Δh in centimeters and fitting an equation to the data so that the head loss in the permeameter can be calculated for different flow rates. The head loss for the measured head, as calculated from the best-fit equation, is then subtracted from the measured head before calculation of hydraulic conductivities. For the empty permeameter, run only with screens (Fig. 6), the best-fit

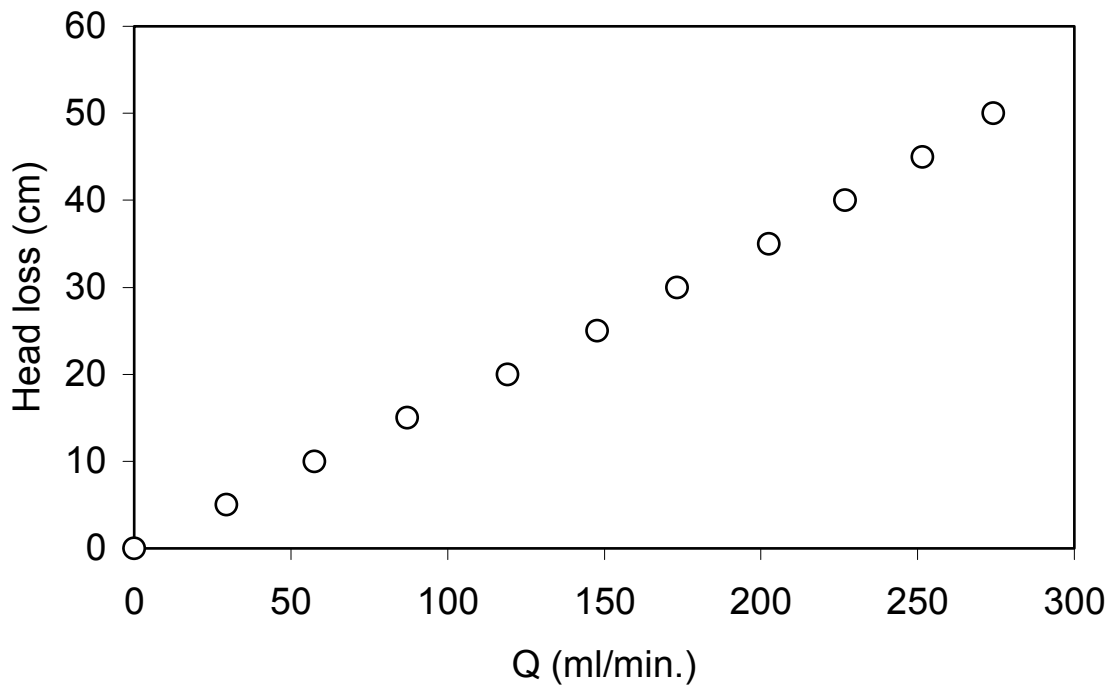


Figure 6. Plot of head loss versus flow rate Q for empty permeameter with stainless steel screens.

equation is

$$\Delta h = -149.93 + 150.29 \exp\left(\frac{-Q}{-966.27}\right) \quad (2)$$

r^2 for this equation is 0.9998. For the empty permeameter run only with porous stones (Fig. 7), the best-fit equation is

$$\Delta h = 0.685 + 0.428Q^{1.5} \quad (3)$$

r^2 for this equation is 0.9909. Nonlinearity of the curve (Fig. 7) may be due to expansion and contraction of flow in the empty permeameter (Burger and Belitz, 1997). The deformation band samples had such low flows that the correction factors calculated by Equation 3 were insignificant.

Possible errors that might cause inaccurate determinations of the hydraulic conductivity include.

1. Inaccurate measurements of volume of discharged water, sample length, cross-sectional area, head difference, etc.
2. Small quantities of air dissolved in the water might tend to collect at the sample-water interface and reduce the apparent hydraulic conductivity over time. De-aired water and vacuum evacuation of the sample prior to saturation were used for this reason.
3. When swelling clays are present, a difference in water quality between the testing solution and the water in an aquifer might cause differences between actual and measured hydraulic conductivities.
4. Differing compaction conditions between the aquifer and the laboratory.

The precision of measurement was ± 0.05 cm for both sample length and diameter, except for the deformation band samples where it was ± 0.02 cm, ± 0.5 seconds (except

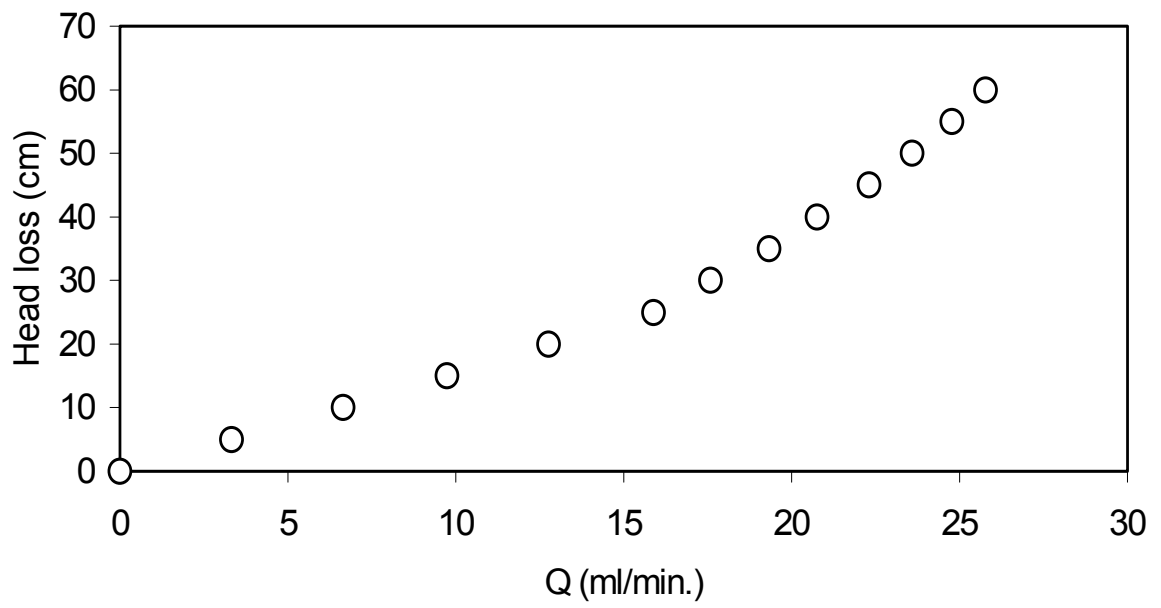


Figure 7. Plot of head loss versus flow rate Q for empty permeameter with porous stones.

when the syringe pump was used), $\pm 0.63 \text{ cm}^3$ for volume (average drop of water), except when the syringe pump was used), and $\pm 0.05 \text{ cm}$ for head measurements (except when using syringe pump). Thus, assuming evaporation to be minimal and ignoring possible problems from air bubbles, the precision of the method can be estimated by calculating the maximum expected hydraulic conductivity from

$$K_{\text{high}} = \frac{(V + 0.63)(L + 0.05)}{\pi(R - 0.05)^2(t - 0.5)(h - 0.05)} \quad (4)$$

where R is the sample radius, and the minimum expected hydraulic conductivity from

$$K_{\text{low}} = \frac{(V - 0.63)(L - 0.05)}{\pi(R + 0.05)^2(t + 0.5)(h + 0.05)} \quad (5)$$

the percentage error E can then be calculated from

$$E = \pm \left(\frac{K_{\text{high}} - K_{\text{low}}}{2K_{\text{average}}} \right) 100 \quad (6)$$

No hydraulic conductivity standards were available to check the permeameter for bias.

The transducer used with the syringe pump has an accuracy of $\pm 0.5 \text{ psi}$. The flow rates and pressures were obtained directly from the instrument, which has a flow error of 1 part in 10,000. Thus, when the syringe pump was used as a constant head source, h was $\pm 30.3 \text{ cm}$. The length of the deformation band samples was measured more carefully so that

$$K_{\text{high}} = \frac{\left(V + \frac{V}{10000} \right) (L + 0.02)}{\pi(R - 0.05)^2(t)(h - 30.3)} \quad (7)$$

and

$$K_{\text{low}} = \frac{\left(V - \frac{V}{10000}\right)(L - 0.02)}{\pi(R + 0.05)^2(t)(h + 30.3)} \quad (8)$$

The head differential measured by the transducer in psi was converted to cm of head using

$$h = \frac{P}{\rho g} \quad (9)$$

The pressure head in psi is first converted to N/m^2 by multiplying by $6.895 \times 10^3 \text{ N/m}^2$, the gravitational constant $g = 9.8 \text{ m/s}^2$, and water density $\rho = 997.538 \text{ Kg/m}^3$ (at 23°C). Head differentials used with the syringe pump ranged from a low of 1,057 to a high of 2891 cm.

The Intrinsic permeability k (Appendix) was calculated in darcies from

$$k = \frac{K\left(\frac{\mu}{\rho g}\right)}{9.87 \cdot 10^{-9}} \quad (10)$$

Where viscosity $\mu = 0.009358 \text{ g/s}\cdot\text{cm}$ (at 23°C)

Where the sample was composed of a layered sandwich of matrix sand and one or more deformation bands oriented perpendicular to flow, the equivalent vertical hydraulic conductivity was calculated from the following equation using the inverse harmonic mean model (Deutsch, 1989) under the assumption that each layer is homogeneous.

$$K_{\text{effective}} = \frac{\sum b_i}{\sum \left(\frac{b_i}{K_i}\right)} \quad (11)$$

where $K_{\text{effective}}$ is the average vertical hydraulic conductivity(cm/s), b_i is the thickness of each layer(cm), and K_i is the vertical hydraulic conductivity of each layer(cm/s).

When the samples consisted of a sandwich of matrix sand and deformation bands oriented parallel to flow, equivalent (average) horizontal hydraulic conductivity can be calculated by an inverse arithmetic mean model (Deutsch, 1989) according to.

$$K_{\text{effective}} = \frac{\sum (b_i K_i)}{\sum b_i} \quad (12)$$

RESULTS

A total of 30 hydraulic conductivity measurements were made; 16 from Site 1 and 14 from Site 2 (Appendix). At Site 1, eight measurements of undeformed sediments and eight measurements of deformed sediments were made. At Site 2, six measurements were from undeformed sediments and eight measurements were from deformed sediments.

Site Description

Site 1.

The whole outcrop covers a vertical distance of about 6 m and consists of eolian sands overlain by fluvial and alluvial fan facies (Fig. 8). The eolian deposits are composed of well- to moderately-sorted, buff to light brown, fine to coarse-grained subangular sands. Large scale cross-stratification (strike N 70°E), tangential foresets (1 to 2 m), and planar bedding and a number of small displacement faults or deformation bands are observable in this outcrop. The eolian facies is composed of two units; an upper part that is about 40 cm thick consisting planar bedded, medium- to fine-grained, well-sorted buff sand; and a lower part which is composed of fine- to coarse-grained, light-brown or gray sand, moderately sorted with large-scale cross-stratification interlayered with coarse layers. Calcareous cemented beds and concretions are present along several horizons at various locations in the railroad cut.

At Site 1, the thickness of individual deformation bands is about 1mm, and they typically have displacements ranging from 3 to 20 mm. The deformation zone also varies

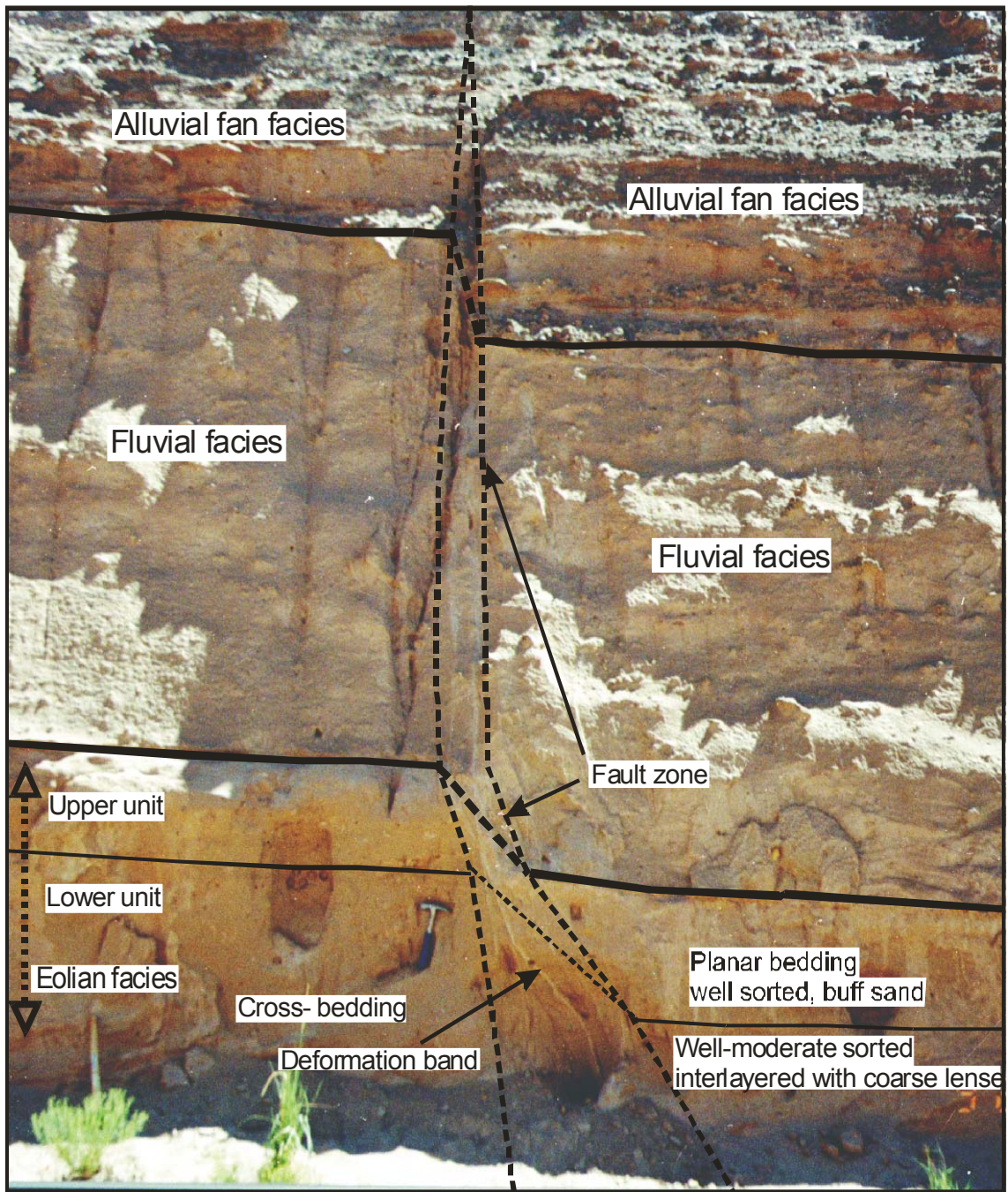


Figure 8. Lithology and structure of site 1.

from 2 mm to 1.5 cm in thickness. The bands are variable in thickness and have a wavy shape rather than planar in plan view. The total vertical displacement in the fault zone is estimated from the displacement of the contact between the eolian and the fluvial facies and is about 53 cm.

Site 2.

This site is located about 20 m south of Site 1 and consists of eolian deposits composed mostly of the upper unit of the eolian facies. The lower eolian unit is buried at this site (Fig. 9). The whole outcrop covers a 5 m vertical section. This site is also overlain by approximately 1 m of an alluvial fan facies and about 1.3 m of a fluvial facies. The eolian facies is characterized by mostly well-sorted, fine-grained, horizontally-laminated buff sand, although in some locations it appears relatively massive. The bedding is accented by clay laminations and calcareous cemented beds oriented parallel to bedding. The thickness of the individual deformation bands is about 1mm with displacements ranging from 1 to 15 mm. The thickness of deformation zone varies from 2 mm to 0.8 cm. The total vertical displacement of the normal fault in fault zone at Site 2 was estimated by displacement of a clay marker bed and is approximately 42 cm.

Hydraulic conductivity measurement

The results of these measurements are summarized in Tables 1, 2, and Figure 12. Table 3 shows a relationship between deformation band thickness and hydraulic conductivity.

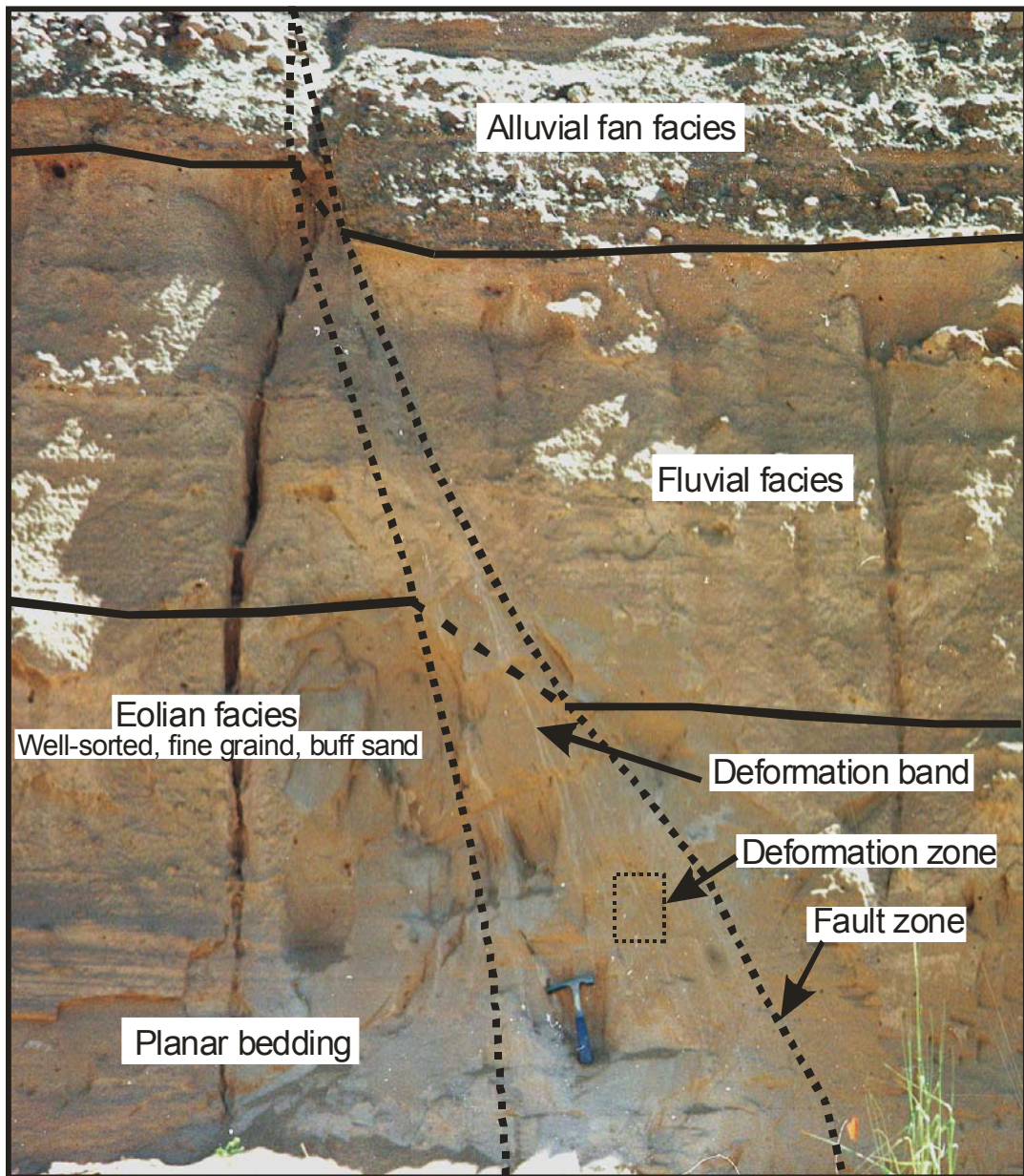


Figure 9. Lithology and structure of Site 2.

Site 1.

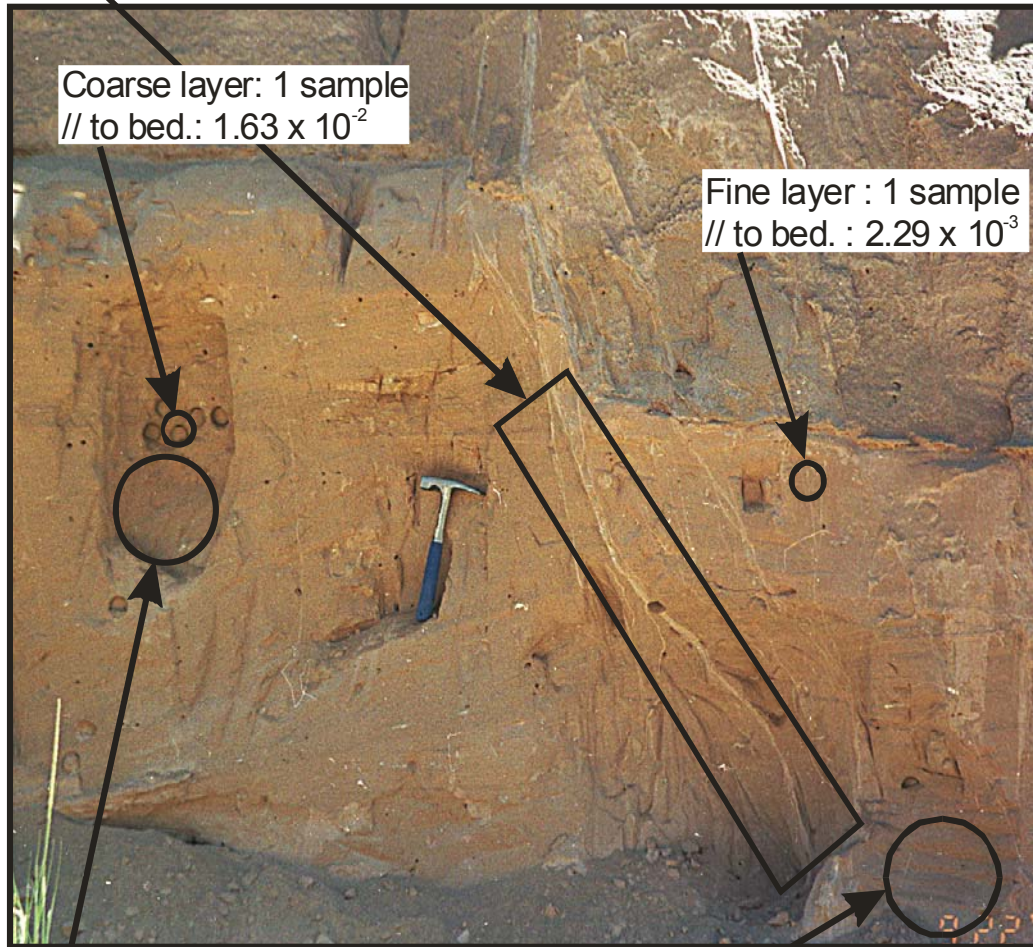
The hydraulic conductivity of undeformed sediments parallel to cross and planar bedding ranged from 2.29×10^{-3} to 1.63×10^{-2} cm/s (Fig. 10). The highest undeformed sand hydraulic conductivity was from the coarse layer within the lower unit and the lowest value was from the upper finer-grained eolian sands. The hydraulic conductivity perpendicular to bedding was not measured in either the coarse or fine layers. The two samples perpendicular to cross-bedding ranged from 6.48 to 6.65×10^{-3} cm/s, yielding a mean ratio between horizontal and vertical hydraulic conductivity of 1.41 for the eolian sand at Site 1. Additionally, in the plane of cross bedding, hydraulic conductivity parallel to the dip direction is a little higher than parallel to strike with a mean ratio of 1.12. In the deformed zone, the hydraulic conductivity perpendicular to the deformation bands, for composite samples containing both deformation bands and undeformed sands, was 3.88×10^{-6} to 3.91×10^{-5} cm/s. Hydraulic conductivity measured parallel to deformation bands in composite samples ranged from 2.56×10^{-4} to 3.71×10^{-3} cm/s. Therefore, there are about two orders of magnitude difference between hydraulic conductivities perpendicular and parallel to deformation bands within the deformed zone. In the samples containing only deformation band material, flow was perpendicular to the band. The hydraulic conductivity of these samples ranged between 2.52 and 3.06×10^{-7} cm/s. The hydraulic conductivity perpendicular to the deformation bands in composite samples, as calculated using the inverse harmonic mean model, ranged from 2.24 to 3.41×10^{-6} cm/s.

Deformation zone : 8 samples

⊥ to homog. def. bands : 3.06×10^{-7} , 2.52×10^{-7}

Def. zone, ⊥ to def. bands : 3.88×10^{-6} , 4.05×10^{-6} , 9.68×10^{-6} , 3.91×10^{-5}

Def. zone, // to def. bands : 2.56×10^{-4} , 3.71×10^{-3}



Site 1a : 3 samples

⊥ to X-bed. : 6.65×10^{-3}

// to strike : 9.09×10^{-3}

// to dip : 9.47×10^{-3}

Site 1b : 3 samples

⊥ to X-bed. : 6.48×10^{-3}

// to strike : 8.47×10^{-3}

// to dip : 1.01×10^{-2}

Figure 10. Location of hydraulic conductivity measurements at Site 1.

(⊥: Perpendicular, //: Parallel, homog.: homogeneous, def.: Deformation, X-bed.: Cross-bedding)

Table 1. Hydraulic conductivity of undeformed sands.

Location	Orientation	Hydraulic conductivity (cm/s)
Site 1a ⁴ (Foot wall)	Normal to bedding	6.65×10^{-3}
	Parallel to Strike	9.09×10^{-3}
	Parallel to dip direction	9.47×10^{-3}
Site 1b ⁵ (Hanging wall)	Normal to bedding	6.48×10^{-3}
	Parallel to Strike	8.47×10^{-3}
	Parallel to dip direction	1.01×10^{-2}
Site 2a	Normal to bedding	2.11×10^{-3}
	Parallel to bedding, XX ¹	2.91×10^{-3}
	Parallel to bedding, YY ²	3.69×10^{-3}
Site 2b	Normal to bedding	2.49×10^{-3}
	Parallel to bedding, XX	3.44×10^{-3}
	Parallel to bedding, YY	3.51×10^{-3}
Site 1	Coarse layer, // ³ to bedding	1.63×10^{-2}
	Finer layer, // to bedding	2.29×10^{-3}

¹Perpendicular to outcrop, ²Parallel to outcrop, ³Parallel, ⁴Foot wall, ⁵Hanging wall

Site 2.

The hydraulic conductivity of four undeformed samples parallel to bedding ranged from 2.91 to 3.69×10^{-3} cm/s (Fig. 11). Perpendicular to bedding the range was 2.11 to 2.49×10^{-3} cm/s, yielding a mean ratio of hydraulic conductivity between parallel and perpendicular to bedding of 1.47 for Site 2. Within the bedding plane, the hydraulic conductivity anisotropy ratio is 1.14.

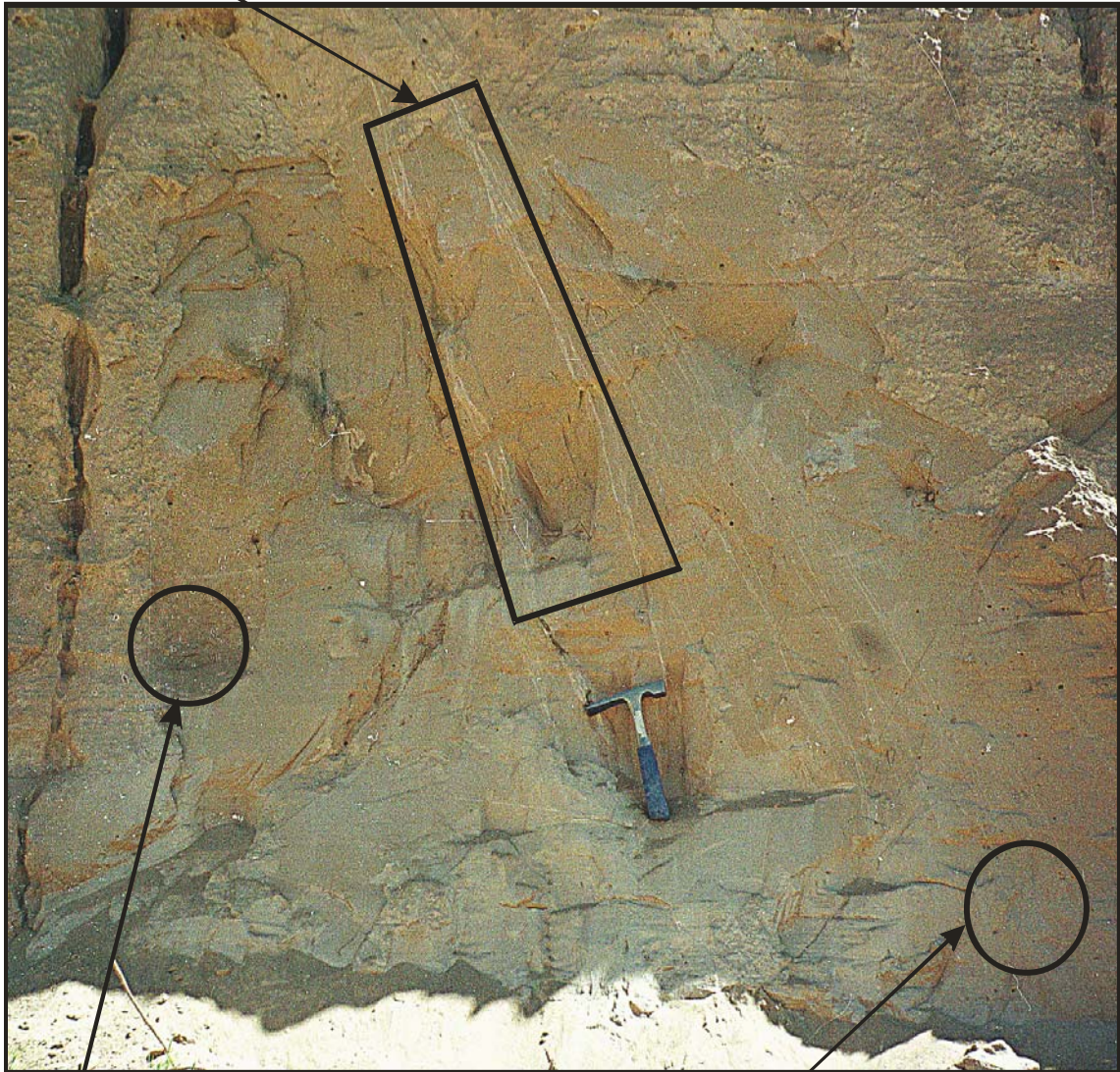
In the deformed zone at Site 2, hydraulic conductivity of composite samples oriented perpendicular to deformation bands ranged from 1.61×10^{-5} to 4.03×10^{-4} cm/s. Parallel to the deformation bands in composite sample, hydraulic conductivity was 1.22 and 2.98×10^{-3} cm/s, respectively. The hydraulic conductivity perpendicular to the

Deformation zone : 8 samples

⊥ to homogeneous def. bands : 3.93×10^{-7} , 2.83×10^{-7}

Def. zone, ⊥ to def. bands : 1.61×10^{-5} , 3.42×10^{-5} , 9.91×10^{-5} , 4.03×10^{-4}

Def. zone, // to def. bands : 1.22×10^{-3} , 2.98×10^{-3}



Site 2a : 3 samples

⊥ to bed. : 2.11×10^{-3}

// to bed. XX : 2.91×10^{-3}

// to bed. YY : 3.69×10^{-3}

Site 2b : 3 samples

⊥ to bed. : 2.49×10^{-3}

// to bed. XX : 3.44×10^{-3}

// to bed. YY : 3.51×10^{-3}

Figure 11. Location of distribution of hydraulic conductivity (cm/s) at Site 2.

Table 2. Hydraulic conductivity of deformed sands.

Sample No.	Sample Location	Orientation	Hydraulic conductivity (cm/s)
A	Site 1	\perp ¹ to homog. ² def. ³ bands	3.06×10^{-7}
B		-	2.52×10^{-7}
C		Def. zone, // ⁴ to bands	3.71×10^{-3}
D		-	2.56×10^{-4}
E		Def. zone, \perp to bands	3.91×10^{-5}
F		-	4.05×10^{-6}
G		-	9.68×10^{-6}
H		-	3.88×10^{-6}
A	Site 2	\perp to homog. def. bands	3.93×10^{-7}
B		-	2.83×10^{-7}
C		Def. zone, // to band	1.22×10^{-3}
D		-	2.98×10^{-3}
E		Def. zone, \perp to band	4.03×10^{-4}
F		-	1.61×10^{-5}
G		-	9.91×10^{-5}
H		-	3.42×10^{-5}

¹Perpendicular, ²Homogeneous, ³Deformation, ⁴Parallel

Table 3. Hydraulic conductivity versus thickness of deformation bands in homogeneous samples.

Thickness of homogeneous deformation bands sample (cm)	Hydraulic conductivity (cm/s)
0.6	3.06×10^{-7}
0.3	2.52×10^{-7}
0.3	3.93×10^{-7}
0.2	2.82×10^{-7}

homogeneous bands was 2.83 and 3.93×10^{-7} cm/s. In composite samples, hydraulic conductivity of perpendicular to the deformation bands calculated using the inverse harmonic mean model ranged from 2.21×10^{-6} to 2.17×10^{-5} .

Hydraulic conductivity of undeformed samples typically decreased about 20 to 30% over 2 to 3 hours and then stabilized at a roughly constant value (Fig. 13). Each test ran for approximately 5 hours. The hydraulic conductivity of deformed sands decreased about 50 to 80% during 4 to 8 hours and then stabilized. These tests were typically run for 10 hours.

Equations 4 through 8 were used to estimate the precision of the hydraulic conductivity measurements. These estimated accuracies ranged from a high of $\pm 33.2\%$ to a low of $\pm 6.7\%$ with a mean of $\pm 13.1\%$. The one-standard deviation analytical precision of replicate steady-state measurements ranged from a high of $\pm 7.9\%$ to a low of $\pm 0\%$, with a mean of $\pm 1.4\%$. For this reason, it is best to use precision estimates developed from error analysis, as in Equations 4 ~ 8 rather than the replicate precision for a single sample in interpreting the results of this study.

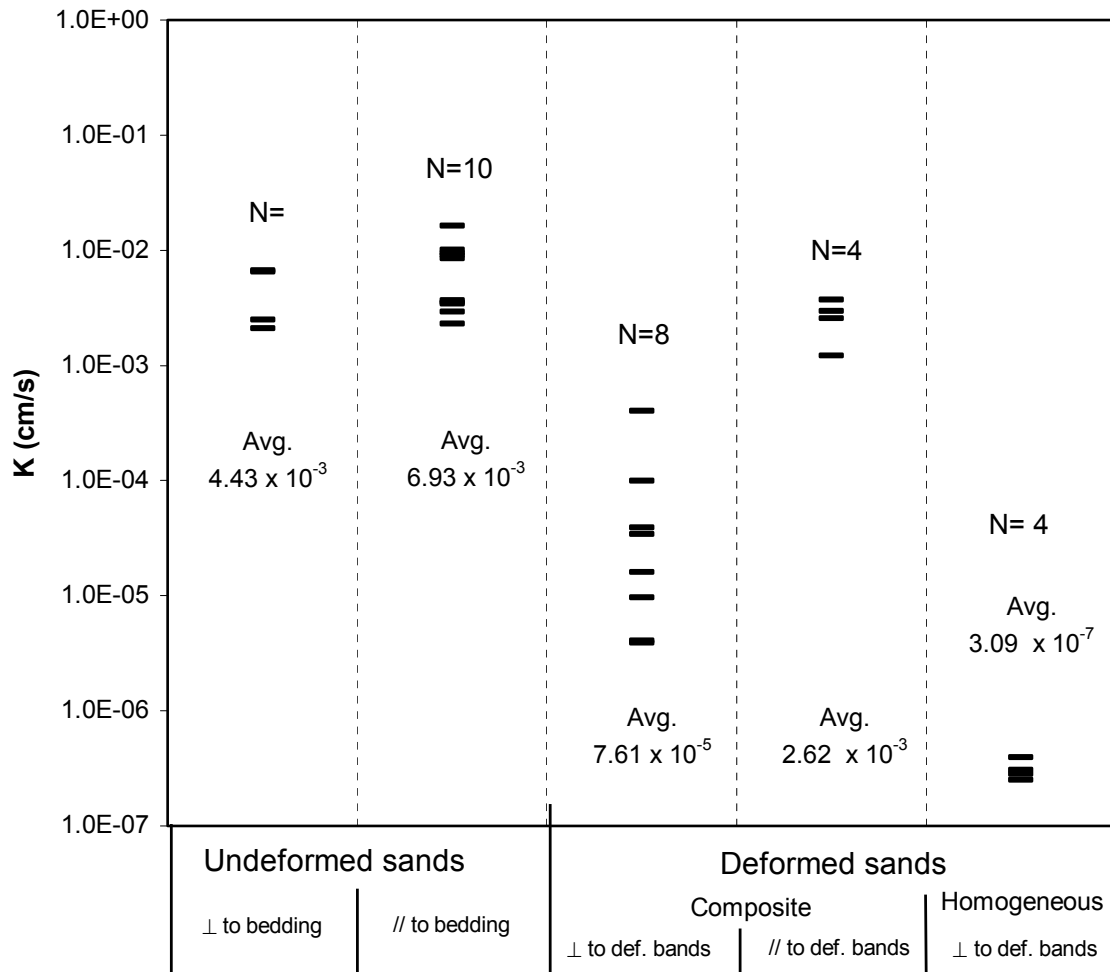


Figure 12. Plot of hydraulic conductivity of all samples.
 (N: number of samples, Avg.: average hydraulic conductivity)

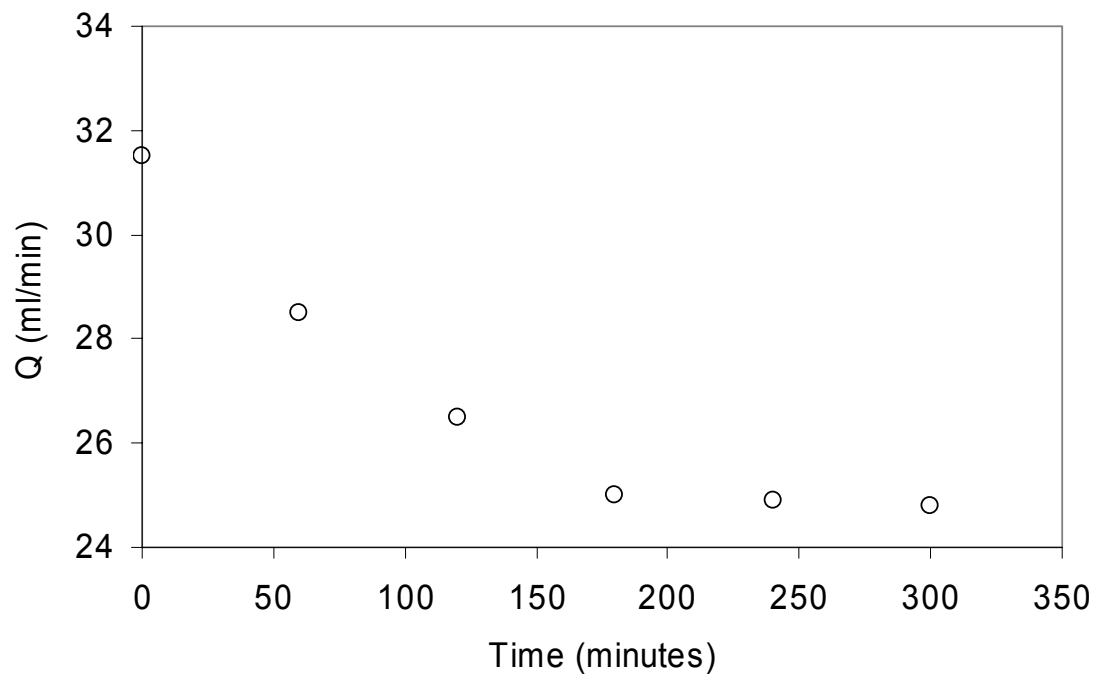


Figure 13. Plot demonstrating the decrease of flow rate Q over time (undeformed sands, perpendicular to bedding, Site 1a). Each sample was run to steady state and the hydraulic conductivity was calculated from a minimum of three steady state readings.

Texture and Mineralogy

Four samples, two of undeformed sands and two of deformation band material (Table 4) were examined to determine the mineral composition (Table 5) and percentage of the clay-size fraction (Table 6). Each sample was disaggregated and the sand and gravel were separated by sieving through a 230-mesh screen, then the clay-size fraction was separated from the remaining samples using a hydrometer, dried, and finally analyzed by X-ray diffraction at the New Mexico Bureau of Mines and Mineral Resources X-ray laboratory. The X-ray diffraction method identifies the clay and other minerals found within the clay-size fraction and provides a semi-quantitative estimate of their abundance. Illite and smectite are present and clinoptilolite (zeolite), feldspar, quartz, and calcite were also identified as clay-size fraction components. The deformed sediments contain larger percentages of smaller grain sizes and exhibit poorer sorting.

Table 4. X-ray diffraction sample description.

Sample ID	Sample Location
GA98063	Undeformed sand of Site 1- footwall block
GA98064	Deformation bands of Site 1
GA98065	Undeformed sand of Site 2- footwall block
GA98066	Deformation bands of Site 2

Table 5. Mineralogy of clay-size fraction.

Sample Location	Illite	Smectite	I/S ¹	Others ²
Undeformed sand Site 1- footwall block	50 ³	50	TR	<u>CLINO</u> , FEL
Site 1, Deformation bands	40	30	30	<u>CLINO</u> , QTZ, FEL, CAL
Undeformed sand Site 2- footwall block	50	20	30	<u>CLINO</u> , QTZ, FEL
Site 2, Deformation bands	20	50	30	CLINO, QTZ, FEL, (CAL)

¹I/S : Mixed-layer illite and smectite clays

²Non-clay minerals : QTZ = quartz, FEL = feldspars; CAL = calcite; CLINO = clinoptilolite, TR = trace or less than 5%, ____ = major component, and () = minor component.

³The results are reported as percent following clay mineral groups: kaolinite, illite, chlorite, smectite, and I/S (mixed-layer illite-smectite)

Table 6. Particle size analysis.

Sample Location	SAND ¹	SILT ²	CLAY ³
Undeformed sand Site 1a - footwall block	95 ⁴	4	1
Site 1, Deformation bands	74	22	4
Undeformed sand Site 2a - footwall block	93	5	2
Site 2, Deformation bands	84	14	3

¹Larger than 1/16 mm, ²2 micron to 1/16 mm, ³Less than 2 micron

⁴Particle size analysis reported as percentage, Results accurate to $\pm 2\%$

DISCUSSION

Haneberg et al., (1998) measured hydraulic conductivity of recompacted samples from the Santa Fe Group, most of which contained more clay than the samples measured in this study, and found that hydraulic conductivity decreases exponentially over time due to secondary consolidation of the sample. In this study, hydraulic conductivity also decreased over time. In a flexible wall permeameter, the sample is under confining pressure and therefore the specimen may compact over time. However, the confining pressure used in this study was low (10 psi, except for the seven deformation band samples) and it is doubtful that such low compaction pressures could cause an extensive decrease in hydraulic conductivity.

The presence of clay in pores and pore throats may affect hydraulic conductivity. All samples contained small amounts of smectite, highly expandable clay. The degree to which smectite swells when in contact with fluids (thereby reducing flow through the sample) is, in part, dependent on fluid chemistry. Morre et al., (1982) found that strong electrolyte solutions suppress the water bonding properties of smectite platelets, and as a result, clay hydraulic conductivities can vary by orders of magnitude in different electrolyte solutions. The fact that different hydraulic conductivity values are often obtained using air versus water may be partially explained by the presence of swelling clays in the pores. Because this study was conducted with tap water, which has its source from local groundwater, the hydraulic conductivities measured in this study should be representative of what might be expected for this facies if it were saturated with groundwater.

Also, air bubbles might be concentrated between water and sample even though degassing was carefully conducted prior to each measurement. However, hydraulic conductivities of all of specimens reached steady state after 2 to 8 hours. Therefore, the values of hydraulic conductivities reported in this study are reasonable.

It has been recognized that the hydraulic conductivity of sands is affected by lithology (grain size, sorting, shape, etc.) and the degree of diagenetic alteration (e.g., compaction and cementation). The directional hydraulic conductivity measurements of undeformed sands, perpendicular to cross- or planar-bedding show lower hydraulic conductivities than parallel to them. Even though grain fabric on foresets is known to be parallel to dip direction (Hamilton et al., 1968), anisotropy is not very high within the plane of bedding in foresets.

The directional anisotropy reported in this study in undeformed sands could be because of preferential grain orientations and bedding or lamination of the sediments during deposition. In a previous study, Potter and Mast (1963) reported that framework grains in sandstone appear to accumulate with their long axes parallel to current flow and imbricate upcurrent 10 to 25 degrees from the depositional interface (Potter and Mast 1963). Mast and Potter (1963) also documented that orientation, packing, and shape of the framework grains have a much stronger effect on vertical hydraulic conductivity than horizontal conductivity. Accordingly, both grain fabric orientation and lamination (bedding) might cause hydraulic conductivity perpendicular to bedding to be less than that parallel to bedding structure.

The results of the hydraulic conductivity measurements in the undeformed sand matrix suggest that vertical hydraulic conductivity (perpendicular to cross stratification or

planar bedding) in the outcrop is about 43% less than the maximum measured hydraulic conductivity, which lies in the plane of bedding. Considering the estimated error of $\pm 10.8\%$ involved in these specific measurements, this is a significant difference. The difference in hydraulic conductivity measured on the axes, which lie in the plane of bedding, was 12.0%. The estimated error for these measurements was $\pm 10.6\%$, thus the measured difference in hydraulic conductivity within the plane of bedding may not be significant.

Does hydraulic conductivity parallel to bedding represent the maximum hydraulic conductivity? Previous studies documented that the maximum hydraulic conductivity may be parallel to the grain orientation rather than parallel to bedding (Griffiths, 1961; Potter and Mast, 1963). Therefore, if angle of the grain imbrication exists and/or is figured out, it is possible to predict the direction of the maximum hydraulic conductivity.

What effect does hydraulic conductivity anisotropy have on water and chemical movement? Since conductivity is greater parallel to than perpendicular to bedding, greater flow of both water and chemicals would be expected parallel to bedding. This suggests that a contaminant plume in these sediments where no deformation bands are encountered would tend to spread more rapidly parallel to bedding. The data in this study suggest that conductivity parallel to dip direction and parallel with bedding might be a little higher than conductivity parallel to strike and parallel to bedding, although the precision of these measurements is not sufficient to prove this point. However, if this is the case, then a contaminant plume in these sediments would be slightly elongate in the direction parallel with bedding and perpendicular to strike, and significantly compressed

perpendicular to bedding, assuming the groundwater flow direction was in the direction of maximum conductivity.

The hydraulic conductivity of deformation bands measured perpendicular to the deformation band ranged from 2.52×10^{-7} to 2.17×10^{-5} cm/s, including the values calculated by the inverse harmonic mean model. The hydraulic conductivity of undeformed sands ranged from 2.11×10^{-3} to 1.63×10^{-2} cm/s. This result suggests that hydraulic conductivity of deformation bands may be more variable than that of the undeformed sands. It is likely dependent on the amount of displacement, deformation band thickness, and grain size within the deformation band.

The shape of the deformation bands is not planar so that flow between the deformation bands can be blocked by eye or ramp structures. Also, additional deformation may occur immediately adjacent to deformation bands. Antonellini and Aydin (1994) calculated hydraulic conductivities in well consolidated sandstones parallel to a deformation band using an arithmetic mean model and their value is about one order of magnitude larger than that perpendicular to the deformation bands. In this study measurements of conductivity parallel to deformation bands proved insensitive.

An important question is what effect do the small, < 1 cm deformation bands commonly found in faulted sediments have on water and chemical movement? Do they significantly slow or redirect water and/or chemical movement, or is their effect negligible? The average hydraulic conductivity across the thin deformation bands measured in this study is 3.1×10^{-7} cm/s. The average hydraulic conductivity of the matrix sands measured in this study is 6.2×10^{-3} cm/s. Thus, there is a four-order of

magnitude decrease in the hydraulic conductivity in the deformation bands or, to put it another way, the sands on average are 20,000 times more permeable than the deformation bands.

Sigda (1997) measured a maximum three-order of magnitude decrease in hydraulic conductivity between the matrix sands and the deformation bands at his study sites in lower Santa Fe Group sediments. This study found a maximum difference of four orders of magnitude. This difference is probably due to three factors. First, Sigda's (1997) faults may not have similar conductivities as those examined in this study. Second, Sigda's (1997) data were obtained with an in-situ air permeameter, so clay swelling in the pores and pore throats during his measurements was not a factor. The hydraulic conductivity measurements performed in this study used the local groundwater and there typically was a decrease in hydraulic conductivity over time of 20 to 30% for the undeformed sands, and 50 to 80% for the deformation band samples. All of the samples contained swelling clays (Table 4). Second, the flexible-wall permeameter used in this study exerts a small compaction pressure on the samples, which the air permeameter does not. Some of the hydraulic conductivity decrease might be due to compaction. Clays tend to be swollen in the pores and pore throats of saturated aquifer sands, and sands at depth tend to be more compacted than in outcrop. Therefore, the four order of magnitude maximum hydraulic conductivity decreases may be closer to what actually occurs in the aquifer.

This difference in hydraulic conductivity suggests that, depending upon the continuity and attitude of the deformation bands, they will 1) act as leaky barriers to flow of water and dissolved chemicals, 2) act as barriers to non-wetting phase fluids, 3)

depending upon geometry and pore size, act as small-scale traps for free-phase nonaqueous phase contaminants, especially at and near the juncture of two or more deformation bands, and 4) discontinuous sections of deformation bands might serve to redirect the flow of water and dissolved contaminants, and/or flow of nonaqueous phase contaminants thus complicating the distribution of contaminants at a site.

Also, water supply wells located near a small, sub-meter scale fault in poorly consolidated sediments will produce less water due to interference of the deformation bands with water flow, than one not located near a fault. Additionally, if a monitoring well is installed in a pump and treat system such that there is even one deformation band located between it and the contaminant plume, the deformation band will reduce the effectiveness of the well in removing the contaminants. Even if the deformation bands are discontinuous, pump and treat systems will have to produce significantly higher volumes of water to impact contaminant levels than if the deformation bands were not present.

The results of this study, and those of Sigda (1997), suggest that small-displacement faults in poorly consolidated sediments may have significant impacts on hydraulic conductivity anisotropy and should not be ignored in relation to water supply and contaminated sites. These small-displacement faults are seldom mapped, even at the site level. However, the results of this study suggest that these effects should be factored into smaller-scale water supply studies and remediation efforts at contaminated sites.

SUMMARY AND CONCLUSIONS

Undisturbed, oriented samples from both undeformed and deformed sediments were collected in the field from eolian facies in the lower Santa Fe Group (middle Miocene to late Oligocene age), and hydraulic conductivities were measured using a flexible-wall permeameter. This eolian facies is characterized by poorly consolidated and well- to moderately-sorted fine- to coarse-grained sand, and large-scale cross stratification and planar bedding. These sediments are cut by deformation bands associated with small faults having typical throws of less than one meter. The deformation bands within the deformed zones exhibit smaller grain size, poorer sorting, and lower hydraulic conductivity than the surrounding undeformed sands.

The experimental results show that the hydraulic conductivity of the undeformed sands is significantly greater parallel to bedding than perpendicular to bedding. The hydraulic conductivity of undeformed sediments parallel to bedding ranged from 2.29×10^{-3} to 1.63×10^{-2} cm/s, and perpendicular to bedding ranged from 2.11×10^{-3} to 6.65×10^{-3} cm/s. The mean ratio for both Sites between hydraulic conductivity parallel to and perpendicular to bedding was 1.43.

The hydraulic conductivity perpendicular to deformation bands is four orders of magnitude less than the undeformed host sediments and ranged from 2.52×10^{-7} to 3.93×10^{-7} cm/s. Hydraulic conductivity perpendicular to deformation bands may depend on the fault displacement, band thickness, and grain size within the band. However, no relationship between deformation band thickness and hydraulic conductivity was discernable from the data.

Both depositional and deformational processes may influence hydraulic conductivity and anisotropy in the faulted poorly consolidated sediments. The major control of anisotropy in the undeformed sands is most likely depositional controls on grain orientation and bedding structure, and hydraulic conductivity reduction in individual deformation bands may be caused by cataclasis, rotation of grain fragments, clay content and diagenetic processes.

The results suggest that a dissolved contaminant plume that encounters no deformation bands in these sediments will tend to spread more rapidly parallel to bedding and have a smaller thickness perpendicular to bedding.

The four-order of magnitude difference between the hydraulic conductivity of the deformation bands and that of the host sands suggests that, depending upon the continuity and attitude of the deformation bands, they might 1) act as leaky barriers to flow of water and dissolved chemicals, 2) act as barriers to free-phase nonaqueous phase contaminant mobility, 3) depending upon geometry and pore size, act as small-scale traps for free-phase nonaqueous phase contaminants, especially at and near the juncture of two or more deformation bands, 4) discontinuous sections of deformation bands might serve to redirect the flow of water and dissolved chemicals, and/or flow of nonaqueous phase contaminants thus complicating the distribution of contaminants at a site.

RECOMMENDATIONS FOR FUTURE WORK

This study has pointed out the important role that small, less than one-meter, scale faults can have on water and chemical movement. Future work should include developing methods to predict the distribution and frequency of these small faults at differing scales so that their impact on water and chemical movement can begin to be quantified. The relationship between deformation band hydraulic conductivity, thickness, throw, sediment mineralogy, grain-size, and pore size need to be quantitatively investigated as well so that predictive models of small-scale fault hydraulic conductivity can be developed if the impact of these small faults is to be understood at larger scales.

Further work using a mini-flexible wall permeameter is needed to better measure three-dimensional hydraulic conductivity within deformation bands which are usually less than one centimeter thick. Preliminary testing using Tool Dip™ (liquid plastic coating compound) to seal the deformation band sample to the permeameter pistons (instead of rubber membrane which are available only in limited size range) suggests use of a mini-flexible wall permeameter is feasible.

REFERENCES

- Anderholm, S. K., 1983, Hydrogeology of the Socorro and La Jencia Basins, Socorro County, New Mexico, Guidebook – New Mexico Geological Society, v. 34, p. 303-310.
- Antonellini, M.P. and Aydin. A., 1994, Effect of faulting on fluid flow in porous sandstones: petrophysical properties, AAPG Bull., v. 78, n. 3, p. 355-377.
- Aydin, A. and Johnson A. M., 1983, Analysis of faulting in porous sandstones, J. Struct. Geol., v. 5, n. 1, p. 19-31.
- Bevan. T. C., 1985, Tectonic evolution of the Isle of Wight: a Cenozoic stress history based on mesofractures, Proc. Geol. Ass.,v. 96, p. 227-235.
- Burger, R. L., and Belitz, K., 1997, Measurement of anisotropic hydraulic conductivity in unconsolidated sands: A case study from a shoreface deposit, Oyster, Virginia, Water Resour. Res., v. 33, p. 1515-1522.
- Cather, S.M., 1992, Suggested revisions to the Tertiary tectonic history of north-central New Mexico, New Mexico Geological Society Guide book, 43rd Field Conference, San Juan Basin IV, p. 109-122.
- Chapin, C. E., and Cather, S. M., 1994, Tectonic setting of the axial basins of the northern and central Rio Grande rift basins of the Rio Grande rift: structure, stratigraphy, and tectonic setting, v. Special Paper 291, p. 5-26.
- Cox, S. F., 1994, Deformation processes and controls on fault mechanics during fault-valve behavior in the Wattle Gully fault zone, central Victoria, Australia in S. Hickman, R. Sibson, and R. Bruhn, eds., The Mechanical Involvement of Fluids in Faulting, USGS Open-file Report 94-228, p. 5-17.
- Davis, J. M., 1994, A Conceptual Sedimentological-Geostatistical Model of Aquifer Heterogeneity Based on Outcrop Studies, Ph.D. Thesis - Jan., 1994.
- Davis, J. M., Wilson, J. L., Phillips, F.M., 1994, A portable air-minipermeameter for rapid in situ field measurements, Groundwater, v. 32, n. 2, p. 258-266.
- Davis, J. M., R. C. Lohman, F.M. Phillips, J.L. Wilson, D.W. Love, 1993, Architecture of the Sierra Ladrones Formation, central New Mexico: Depositional controls on the permeability correlation structure, GSA. Bull., v. 105, p. 998-1007.
- Davis, S. N., and DeWeist, R. J. M., 1966, Hydrogeology, John Wiley, New York.

- Deutsch, C., 1989, Calculating effective absolute permeability in sandstone/shale sequences, SPE Formation Evaluation, v. 4, p. 343-348.
- Fondeur, C., 1964, Etude Petrographique detaillee dun gres a Structure en feuilletts, Rev. Inst. Francais Petrole, v. 19, p. 901-920.
- Gibson, R.G., 1994, Fault zone seals in siliclastic strata of the Columbus Basin, offshore Trinidad, AAPG Bull., v. 78, p. 1372-1385.
- Greenkorn, R.A., Johnson, C.R., and Shallenberger, L.K., 1964, Directional permeability of heterogeneous anisotropic porous media, SPE Journal, v. 4, n. 2, p.124-132.
- Griffiths, J.C., 1961, Measurement of the properties of sediments, J. Geol., v. 69, p. 487-498.
- Hamilton, N., Owens, W.H., and Rees, A. I., 1968, Laboratory experiments on the production of grain orientation in shearing sand, J. Geol., v. 76, p. 465-472.
- Haneberg, W.C., 1995, Steady-state groundwater flow across idealized faults, Water Resour. Res., v. 31, p. 1815-1820.
- Haneberg, W.C., Gomez, P, Gibson, A, and Allred, B., 1998, Preliminary measurements of stress-dependent hydraulic conductivity of Santa Fe Group aquifer system sediments from the 98th St core hole, Albuquerque, New Mexico: New Mexico Geology, v. 20, n. 1, p. 14-20.
- Hardmann, R.F.P., and Booth, J. E., 1991, The significance of normal faults in the exploration and production of North Sea hydrocarbons, Geological Society Special Publication, v. 56, p. 1-13.
- Hawley, J. W., Haase, C.S. and Lozinsky, R.P., 1995, An underground view of the Albuquerque Basin, in Orgega-Klett, C.T., ed., Proceedings of the 39th Annual Water Conference, "The Water Future of Albuquerque and the Middle Rio Grande Basin.", New Mexico Water Resources Institute (in press).
- Huntoon, P. A., and Lundy, D. A., 1979, Fracture-controlled ground-water circulation and well siting in the vicinity of Laramie, Wyoming, Ground Water, v. 17, p. 463-469
- Hutta, J. J., 1956, Relationship of dimensional orientation of quartz grains to directional permeability in sandstone, Pennsylvania State Univ., Coll, Min. Ind., 97 p.
- King, F. H., 1899, Principles and conditions of the movement of groundwater, U.S.G.S., 19th An. Report, 1898-1899, p. 59-94.

- Kelley, V. C., 1977, Geology of Albuquerque Basin, Mem. N. M. Bur. Mines Miner. Resour., v. 33.
- Killey, R. W.D., and Moltyaner, G. L., 1988, Twin Lake tracer tests: Setting, methodology, and hydraulic conductivity distribution, Water Resour. Res., v. 24, n. 10, p. 1585-1612.
- Knipe, R. J., 1993, The Influence of fault zone processes and diagenesis on fluid flow, in Diagenesis and Basin Development, edited by A. D. Hornbury and A. G. Robinson, AAPG Stud. Geol., v. 36, p. 135-148.
- Knipe, R. J. and McCaig, A.M., 1994, Microstructural and microchemical consequences of fluid flow in deforming rocks, in J. Parnell, ed., Geofluids; Origin, Migration and Evolution of Fluids in Sedimentary Basins, GSA Special. Pub., n. 78, p. 99-111.
- Lozinsky, R. .P. and Tedford, R.H., 1991, Geology and Paleontology of the Santa Fe Group, Southern Albuquerque Basin, Valencia County, New Mexico, New Mexico Bureau of Mines and Mineral Resour. Bull., v. 137, p. 157-162.
- Maclay, R.W., and Small, T.A., 1983, Hydrostratigraphic subdivisions and fault barriers of the Edwards aquifer, south-central Texas, USA, J. Hydrology, v. 61, p. 127-146.
- Mast, R.F., and Potter P.E., 1963, Sedimentary structures, sand shape fabrics, and permeability. II, J. Geol., v. 71, p. 548-565.
- Morre, D. E., Morrow, C.A., and Byerlee, J. D., 1982, Use of swelling clays to reduce permeability and its potential application to nuclear waste repository sealing, Geophy. Res. Lett., 9, p. 1009-1012.
- Morrow, C. A., Shi, L. Q., and Byerlee, J.D., 1984, Permeability of fault gouge under confining pressure and shear stress, J. Geophysical Res., v. 89, p. 3193-3200.
- Mozley, P. S., and Goodwin, L., 1995, Patterns of cementation along a Cenozoic normal fault; A record of paleoflow orientations, Geology, v. 23, p. 539-542.
- Nelson, R. A., 1985, Geologic Analysis of Naturally Fractured Reservoirs, Gulf Publishing Company, Houston.
- Neuman, S. P., 1990, Universal scaling of hydraulic conductivities and dispersivities in geologic media, Water Resour. Res., v. 26, p. 1749-1758.
- Pittman, E. D., 1981, Effect of fault-related granulation on porosity and permeability of quartz sandstones, Simpson Group (Ordovician), Oklahoma, AAPG Bull., v. 65, p. 2381-2387.

Potter, P. E., and Mast, R. F., 1963, Sedimentary structures, sand shape fabrics, and permeability. I, *J. Geol.*, v. 71, p. 441-471.

Sigda, J. M., 1997, Effects of small-displacement faults on the permeability distribution of poorly consolidated Santa Fe group sands, Rio Grande rift, New Mexico, MS thesis, New Mexico Institute of Mining and Technology, 105 pp.

Smith, D. A., 1980, Sealing and nonsealing faults in Louisiana Gulf Coast salt basin, *AAPG Bull.*, v. 64, p. 145-172.

APPENDIX

Site 1 - a: Foot-wall, b: Hanging-wall

Undeformed sands

Perpendicular to bedding, Parallel to strike and dip direction

Deformed sands

Perpendicular and Parallel deformation zone (composite sample)

Perpendicular to deformation bands (homogeneous sample)

Site 2 - a: Foot-wall, b: Hanging-wall

Undeformed sands

Perpendicular to bedding, Parallel to bedding

[XX (perpendicular to outcrop), and YY (parallel to outcrop) orientation]

Deformed sands

Perpendicular and Parallel to deformation bands (composite sample)

Perpendicular to deformation bands (homogeneous sample)

KEY to Data Tables

Description of abbreviations:

A	Cross-section area of sample cylinder (cm ²)
Chm-P	Chamber pressure in permeameter (psi)
Elp-time	Elapsed time of measurement (minute)
Flowrate	Rate of water flow through sample (ml/min.)
H	Hydraulic head difference (cm)
H-corret.	Correction factor of hydraulic head (cm)
k	Intrinsic permeability (darcies)
k _{avg}	Average intrinsic permeability (darcies)
K	Hydraulic conductivity (cm/s)
K _{def.}	Hydraulic conductivity of deformation bands (cm/s)
K _{avg}	Average hydraulic conductivity (cm/s)
L	Length of the specimen (cm)
P-head	Pressure head (psi)
P-head.corret	Correction factor of pressure head (psi)
T	Length of time of flow (second)
Temp.	Temperature of discharged water (Celsius)
V	Volume of water percolated (cm ³)

KEY to Graph

Description of abbreviations:

Dip.	Dip direction
Elapsed time	Elapsed time of hydraulic conductivity measurement (minute)
Nor.	Perpendicular to bedding
Pa.	Parallel to bedding
S. #1	Site 1
S. #2	Site 2
Stk.	Strike
Dip.	Dip direction
XX	Perpendicular to outcrop
YY	Parallel to outcrop
//	Parallel
⊥	Perpendicular

Table A1. Site 1a, hydraulic conductivity and permeability data for undeformed sand; perpendicular to bedding.

H [cm]	A [cm ²]	T [minute]	Chm-P [psi]	L [cm]	Elp-time [min.]	H-corret. [psi]	V [cm ³]	K [cm/s]	k [darcies]
10	11.401	1	10	1.6	0	6.00	23.06	8.99E-03	8.72
10	11.401	1	10	1.6	60	6.24	21.53	8.07E-03	7.83
10	11.401	1	10	1.6	120	6.46	20.17	7.30E-03	7.08
10	11.401	1	10	1.6	180	6.61	19.24	6.81E-03	6.60
10	11.401	1	10	1.6	240	6.68	18.78	6.58E-03	6.38
10	11.401	1	10	1.6	300	6.69	18.75	6.56E-03	6.36
Temp. 23° Average Steady State Measurement								6.65E-03	6.45
Single sample replicate precision at one standard deviation ±1.40E-04 or ±2.11 %						Precision estimated from error analysis ±11.3 %			

Table A2. Site 1a, hydraulic conductivity and permeability data for undeformed sand; parallel to strike.

H [cm]	A [cm ²]	T [minute]	Chm-P [psi]	L [cm]	Elp-time [min.]	H-corret. [psi]	V [cm ³]	K [cm/s]	k [darcies]
10	11.401	1	10	1.4	0	4.61	31.77	1.41E-02	13.36
10	11.401	1	10	1.4	60	5.14	28.42	1.13E-02	10.71
10	11.401	1	10	1.4	120	5.48	26.34	9.84E-03	9.33
10	11.401	1	10	1.4	180	5.66	25.21	9.12E-03	8.64
10	11.401	1	10	1.4	240	5.67	25.16	9.08E-03	8.61
10	11.401	1	10	1.4	300	5.67	25.12	9.07E-03	8.60
Temp. 24° Average Steady State Measurement								9.09E-03	8.62
Single sample replicate precision at one standard deviation ±2.49E-05 or ±0.27 %						Precision estimated from error analysis ±11.1 %			

Table A3. Site 1a, hydraulic conductivity and permeability data for undeformed sand; parallel to dip direction.

H [cm]	A [cm ²]	T [minute]	Chm-P [psi]	L [cm]	Elp-time [min.]	H-corret. [psi]	V [cm ³]	K [cm/s]	k [darcies]
10	11.401	1	10	2.3	0	5.65	25.24	1.50E-02	14.57
10	11.401	1	10	2.3	60	6.09	22.53	1.24E-02	12.06
10	11.401	1	10	2.3	120	6.63	19.12	9.70E-03	9.40
10	11.401	1	10	2.3	180	6.67	18.83	9.49E-03	9.21
10	11.401	1	10	2.3	240	6.68	18.81	9.47E-03	9.18
10	11.401	1	10	2.3	300	6.68	18.78	9.45E-03	9.17
Temp. 23° Average Steady State Measurement								9.47E-03	9.19
Single sample replicate precision at one standard deviation ±1.99E-05 or ±0.21 %						Precision estimated from error analysis ±10.5 %			

Table A4. Site 1b, hydraulic conductivity and permeability data for undeformed sand; perpendicular to bedding.

H [cm]	A [cm ²]	T [minute]	Chm-P [psi]	L [cm]	Elp-time [min.]	H-corret. [psi]	V [cm ³]	K [cm/s]	k [darcies]
10	11.401	1	10	1.7	0	6.03	22.89	9.43E-03	9.36
10	11.401	1	10	1.7	60	6.36	20.82	8.14E-03	8.08
10	11.401	1	10	1.7	120	6.65	18.98	7.09E-03	7.04
10	11.401	1	10	1.7	180	6.82	17.91	6.53E-03	6.48
10	11.401	1	10	1.7	240	6.84	17.77	6.46E-03	6.41
10	11.401	1	10	1.7	300	6.84	17.75	6.45E-03	6.40
Temp. 22° Average Steady State Measurement								6.48E-03	6.43
Single sample replicate precision at one standard deviation ±4.26E-05 or ±0.66 %						Precision estimated from error analysis ±11.3 %			

Table A5. Site 1b, hydraulic conductivity and permeability data for undeformed sand; parallel to strike.

H [cm]	A [cm ²]	T [minute]	Chm-P [psi]	L [cm]	Elp-time [min.]	H-corret. [psi]	V [cm ³]	K [cm/s]	k [darcies]
10	11.401	1	10	1.5	0	4.70	31.21	1.46E-02	14.12
10	11.401	1	10	1.5	60	5.08	28.81	1.24E-02	12.06
10	11.401	1	10	1.5	120	5.32	27.31	1.13E-02	10.92
10	11.401	1	10	1.5	180	5.79	24.41	9.24E-03	8.97
10	11.401	1	10	1.5	240	6.09	22.52	8.11E-03	7.86
10	11.401	1	10	1.5	300	6.10	22.41	8.06E-03	7.81
Temp. 23° Average Steady State Measurement								8.47E-03	8.21
Single sample replicate precision at one standard deviation ±6.72E-04 or ±7.93 %						Precision estimated from error analysis ±10.8 %			

Table A6. Site 1b, hydraulic conductivity and permeability data for undeformed sand; parallel to dip direction.

H [cm]	A [cm ²]	T [minute]	Chm-P [psi]	L [cm]	Elp-time [min.]	H-corret. [psi]	V [cm ³]	K [cm/s]	k [darcies]
10	11.401	1	10	2.1	0	5.41	26.77	1.52E-02	14.73
10	11.401	1	10	2.1	60	5.85	24.03	1.26E-02	12.23
10	11.401	1	10	2.1	120	6.12	22.32	1.12E-02	10.86
10	11.401	1	10	2.1	180	6.25	21.52	1.06E-02	10.25
10	11.401	1	10	2.1	240	6.41	20.49	9.81E-03	9.52
10	11.401	1	10	2.1	300	6.41	20.48	9.81E-03	9.51
Temp. 23° Average Steady State Measurement								1.01E-02	9.76
Single sample replicate precision at one standard deviation ±4.36E-04 or ±4.32 %						Precision estimated from error analysis ±10.2 %			

Table A7. Site 2a, hydraulic conductivity and permeability data for undeformed sand; perpendicular to bedding.

H [cm]	A [cm ²]	T [minute]	Chm-P [psi]	L [cm]	Elp-time [min.]	H-corret. [psi]	V [cm ³]	K [cm/s]	k [darcies]
10	11.401	1	10	2.3	0	8.42	7.74	3.09E-03	3.07
10	11.401	1	10	2.3	60	8.55	6.93	2.73E-03	2.71
10	11.401	1	10	2.3	120	8.71	5.93	2.29E-03	2.27
10	11.401	1	10	2.3	180	8.76	5.62	2.16E-03	2.14
10	11.401	1	10	2.3	240	8.78	5.45	2.09E-03	2.07
10	11.401	1	10	2.3	300	8.78	5.44	2.08E-03	2.06
Temp. 22° Average Steady State Measurement								2.11E-03	2.09
Single sample replicate precision at one standard deviation ±4.16E-05 or ±1.97%						Precision estimated from error analysis ± 18.0%			

Table A8. Site 2a, hydraulic conductivity and permeability data for undeformed sand; parallel to bedding, XX orientation.

H [cm]	A [cm ²]	T [minute]	Chm-P [psi]	L [cm]	Elp-time [min.]	H-corret. [psi]	V [cm ³]	K [cm/s]	k [darcies]
10	11.401	1	10	2.1	0	8.14	9.56	3.61E-03	3.58
10	11.401	1	10	2.1	60	8.25	8.82	3.28E-03	3.26
10	11.401	1	10	2.1	120	8.32	8.41	3.10E-03	3.08
10	11.401	1	10	2.1	180	8.36	8.17	3.00E-03	2.98
10	11.401	1	10	2.1	240	8.40	7.88	2.88E-03	2.86
10	11.401	1	10	2.1	300	8.41	7.82	2.85E-03	2.83
Temp. 22° Average Steady State Measurement								2.91E-03	2.89
Single sample replicate precision at one standard deviation ±7.78E-05 or ±2.67%						Precision estimated from error analysis ±14.9%			

Table A9. Site 2a, hydraulic conductivity and permeability data for undeformed sand; parallel to bedding, YY orientation.

H [cm]	A [cm ²]	T [minute]	Chm-P [psi]	L [cm]	Elp-time [min.]	H-corret. [psi]	V [cm ³]	K [cm/s]	k [darcies]
10	11.401	1	10	2.6	0	7.97	10.64	5.07E-03	4.92
10	11.401	1	10	2.6	60	8.16	9.43	4.39E-03	4.26
10	11.401	1	10	2.6	120	8.24	8.89	4.10E-03	3.98
10	11.401	1	10	2.6	180	8.34	8.29	3.78E-03	3.66
10	11.401	1	10	2.6	240	8.37	8.05	3.66E-03	3.55
10	11.401	1	10	2.6	300	8.38	8.04	3.65E-03	3.54
Temp. 23° Average Steady State Measurement								3.69E-03	3.58
Single sample replicate precision at one standard deviation ±7.34E-05 or ±1.99%						Precision estimated from error analysis ±14.2%			

Table A10. Site 2b, hydraulic conductivity and permeability data for undeformed sand; perpendicular to bedding.

H [cm]	A [cm ²]	T [minute]	Chm-P [psi]	L [cm]	Elp-time [min.]	H-corret. [psi]	V [cm ³]	K [cm/s]	k [darcies]
10	11.401	1	10	2.2	0	8.26	8.81	3.43E-03	3.33
10	11.401	1	10	2.2	60	8.45	7.54	2.87E-03	2.78
10	11.401	1	10	2.2	120	8.57	6.83	2.56E-03	2.49
10	11.401	1	10	2.2	180	8.59	6.67	2.50E-03	2.42
10	11.401	1	10	2.2	240	8.59	6.67	2.50E-03	2.42
10	11.401	1	10	2.2	300	8.59	6.65	2.49E-03	2.41
Temp. 23° Average Steady State Measurement								2.49E-03	2.42
Single sample replicate precision at one standard deviation ±4.32E-06 or ±0.17%						Precision estimated from error analysis ±16.5%			

Table A11. Site 2b, hydraulic conductivity and permeability data for undeformed sand; parallel to bedding, XX orientation.

H [cm]	A [cm ²]	T [minute]	Chm-P [psi]	L [cm]	Elp-time [min.]	H-corret. [psi]	V [cm ³]	K [cm/s]	k [darcies]
10	11.401	1	10	2.1	0	7.84	11.46	4.49E-03	4.26
10	11.401	1	10	2.1	60	7.95	10.78	4.16E-03	3.94
10	11.401	1	10	2.1	120	8.07	10.01	3.81E-03	3.61
10	11.401	1	10	2.1	180	8.19	9.22	3.46E-03	3.28
10	11.401	1	10	2.1	240	8.20	9.19	3.44E-03	3.26
10	11.401	1	10	2.1	300	8.20	9.17	3.43E-03	3.25
Temp. 24° Average Steady State Measurement								3.44E-03	3.26
Single sample replicate precision at one standard deviation ±1.17E-05 or ±0.34%						Precision estimated from error analysis ±14.0%			

Table A12. Site 2b, hydraulic conductivity and permeability data for undeformed sand; parallel to bedding, YY orientation.

H [cm]	A [cm ²]	T [minute]	Chm-P [psi]	L [cm]	Elp-time [min.]	H-corret. [psi]	V [cm ³]	K [cm/s]	k [darcies]
10	11.401	1	10	2.4	0	7.90	11.05	4.91E-03	4.87
10	11.401	1	10	2.4	60	8.00	10.44	4.58E-03	4.55
10	11.401	1	10	2.4	120	8.19	9.21	3.95E-03	3.92
10	11.401	1	10	2.4	180	8.33	8.35	3.52E-03	3.49
10	11.401	1	10	2.4	240	8.33	8.33	3.51E-03	3.48
10	11.401	1	10	2.4	300	8.33	8.32	3.50E-03	3.47
Temp. 22° Average Steady State Measurement								3.51E-03	3.48
Single sample replicate precision at one standard deviation ±6.43E-06 or ±0.18%						Precision estimated from error analysis ±14.4%			

Table A13. Site 1, hydraulic conductivity and permeability data for undeformed sand; upper fine layer, parallel to bedding.

H [cm]	A [cm ²]	T [minute]	Chm-P [psi]	L [cm]	Elp-time [min.]	H-corret. [psi]	V [cm ³]	K [cm/s]	k [darcies]
10	11.401	1	10	1.4	0	7.87	11.28	2.93E-03	2.84
10	11.401	1	10	1.4	60	8.02	10.32	2.63E-03	2.55
10	11.401	1	10	1.4	120	8.06	10.02	2.54E-03	2.47
10	11.401	1	10	1.4	180	8.17	9.34	2.34E-03	2.27
10	11.401	1	10	1.4	240	8.21	9.09	2.27E-03	2.20
10	11.401	1	10	1.4	300	8.22	9.05	2.25E-03	2.19
Temp. 23° Average Steady State Measurement								2.29E-03	2.22
Single sample replicate precision at one standard deviation ±4.67E-05 or ±2.04%						Precision estimated from error analysis ±15.1%			

Table A14. Site 1, hydraulic conductivity and permeability data for undeformed sand; intercalated coarse lens, parallel to bedding.

H [cm]	A [cm ²]	T [minute]	Chm-P [psi]	L [cm]	Elp-time [min.]	H-corret. [psi]	V [cm ³]	K [cm/s]	k [darcies]
10	11.401	1	10	2.6	0	4.97	29.53	2.26E-02	21.90
10	11.401	1	10	2.6	60	5.34	27.21	1.94E-02	18.78
10	11.401	1	10	2.6	120	5.62	25.46	1.72E-02	16.70
10	11.401	1	10	2.6	180	5.72	24.84	1.65E-02	16.01
10	11.401	1	10	2.6	240	5.73	24.47	1.62E-02	15.74
10	11.401	1	10	2.6	300	5.73	24.43	1.62E-02	15.72
Temp. 23° Average Steady State Measurement								1.63E-02	15.82
Single sample replicate precision at one standard deviation ±1.67E-04 or ±1.02%						Precision estimated from error analysis ±9.8%			

Table B1. Site 1, hydraulic conductivity and permeability data for deformation band; perpendicular to deformation band; sample A.

P-head [psi]	P-head.corret.. [psi]	L [cm]	A [cm ²]	Chm-P [psi]	Flowrate [ml/min.]	Elp-time [min.]	K [cm/s]	k [darcies]
15	14.98	0.6	11.401	50	1.00	0	8.30E-07	8.05E-04
18	17.98	0.6	11.401	50	1.00	60	6.91E-07	6.71E-04
21	20.98	0.6	11.401	50	1.00	120	5.93E-07	5.75E-04
25	24.98	0.6	11.401	50	1.00	180	4.98E-07	4.83E-04
29	28.98	0.6	11.401	50	1.00	240	4.29E-07	4.16E-04
32	31.98	0.6	11.401	50	1.00	300	3.89E-07	3.77E-04
35	34.98	0.6	11.401	50	1.00	360	3.55E-07	3.45E-04
38	37.98	0.6	11.401	50	1.00	420	3.27E-07	3.18E-04
40	39.98	0.6	11.401	50	1.00	480	3.11E-07	3.02E-04
41	40.98	0.6	11.401	50	1.00	540	3.03E-07	2.94E-04
41	40.98	0.6	11.401	50	1.00	600	3.03E-07	2.94E-04
Temp. 23° Average Steady State Measurement							3.06E-07	2.97E-04
Single sample replicate precision at one standard deviation ±4.38E-09 or ±1.43%					Precision estimated from error analysis ±7.2%			

Table B2. Site 1, hydraulic conductivity and permeability data for deformation band; perpendicular to deformation band; sample B.

P-head [psi]	P-head.corret.. [psi]	L [cm]	A [cm ²]	Chm-P [psi]	Flowrate [ml/min.]	Elp-time [min.]	K [cm/s]	k [darcies]
10	9.98	0.3	11.401	50	1.00	0	6.23E-07	5.90E-04
12	11.98	0.3	11.401	50	1.00	60	5.19E-07	4.92E-04
15	14.98	0.3	11.401	50	1.00	120	4.15E-07	3.93E-04
17	16.98	0.3	11.401	50	1.00	180	3.66E-07	3.47E-04
19	18.98	0.3	11.401	50	1.00	240	3.28E-07	3.10E-04
20	19.98	0.3	11.401	50	1.00	300	3.11E-07	2.95E-04
22	21.98	0.3	11.401	50	1.00	360	2.83E-07	2.68E-04
23	22.98	0.3	11.401	50	1.00	420	2.71E-07	2.56E-04
24	23.98	0.3	11.401	50	1.00	480	2.59E-07	2.46E-04
25	24.98	0.3	11.401	50	1.00	540	2.49E-07	2.36E-04
25	24.98	0.3	11.401	50	1.00	600	2.49E-07	2.36E-04
Temp. 24° Average Steady State Measurement							2.52E-07	2.39E-04
Single sample replicate precision at one standard deviation ±5.99E-09 or ±2.38%					Precision estimated from error analysis ±10.9%			

Table B3. Site 2, hydraulic conductivity and permeability data for deformation band; perpendicular to deformation band; sample A.

P-head [psi]	P-head.corret.. [psi]	L [cm]	A [cm ²]	Chm-P [psi]	Flowrate [ml/min.]	Elp-time [min.]	K [cm/s]	k [darcies]
9	8.97	0.3	11.401	50	2.00	0	1.39E-06	1.38E-03
11	10.97	0.3	11.401	50	2.00	60	1.13E-06	1.13E-03
15	14.97	0.3	11.401	50	2.00	120	8.31E-07	8.25E-04
18	17.97	0.3	11.401	50	2.00	180	6.92E-07	6.87E-04
21	20.97	0.3	11.401	50	2.00	240	5.93E-07	5.89E-04
24	23.97	0.3	11.401	50	2.00	300	5.19E-07	5.15E-04
27	26.97	0.3	11.401	50	2.00	360	4.61E-07	4.58E-04
29	28.97	0.3	11.401	50	2.00	420	4.29E-07	4.26E-04
31	30.97	0.3	11.401	50	2.00	480	4.02E-07	3.99E-04
32	31.97	0.3	11.401	50	2.00	540	3.89E-07	3.86E-04
32	31.97	0.3	11.401	50	2.00	600	3.89E-07	3.86E-04
Temp. 22° Average Steady State Measurement							3.93E-07	3.90E-04
Single sample replicate precision at one standard deviation ±7.25E-09 or ±1.84%					Precision estimated from error analysis ±10.8%			

Table B4. Site 2, hydraulic conductivity and permeability data for deformation band; perpendicular to deformation band; sample B.

P-head [psi]	P-head.corret.. [psi]	L [cm]	A [cm ²]	Chm-P [psi]	Flowrate [ml/min.]	Elp-time [min.]	K [cm/s]	k [darcies]
4	3.98	0.2	11.401	40	1.00	0	1.04E-06	1.01E-03
5	4.98	0.2	11.401	40	1.00	60	8.32E-07	8.07E-04
7	6.98	0.2	11.401	40	1.00	120	5.93E-07	5.76E-04
9	8.98	0.2	11.401	40	1.00	180	4.61E-07	4.47E-04
11	10.98	0.2	11.401	40	1.00	240	3.77E-07	3.66E-04
12	11.98	0.2	11.401	40	1.00	300	3.46E-07	3.35E-04
14	13.98	0.2	11.401	40	1.00	360	2.96E-07	2.87E-04
14	13.98	0.2	11.401	40	1.00	420	2.96E-07	2.87E-04
14	13.98	0.2	11.401	40	1.00	480	2.96E-07	2.87E-04
15	14.98	0.2	11.401	40	1.00	540	2.77E-07	2.68E-04
15	14.98	0.2	11.401	40	1.00	600	2.77E-07	2.68E-04
Temp. 23° Average Steady State Measurement							2.83E-07	2.75E-04
Single sample replicate precision at one standard deviation ±1.14E-08 or ±4.03%						Precision estimated from error analysis ±15.5%		

Table C1. Site 1, hydraulic conductivity and permeability data for deformation zone; parallel to deformation bands (0.3cm) and normal to bedding; sample C.

H [cm]	A [cm ²]	T [minute]	Chm-P [psi]	L [cm]	Elp-time [min.]	H-corret. [psi]	V [cm ³]	K [cm/s]	k [darcies]
10	11.401	1	10	1.9	0	7.32	14.76	5.60E-03	5.43
10	11.401	1	10	1.9	60	7.54	13.37	4.93E-03	4.78
10	11.401	1	10	1.9	120	7.69	12.41	4.48E-03	4.35
10	11.401	1	10	1.9	180	7.91	11.02	3.87E-03	3.75
10	11.401	1	10	1.9	240	7.95	10.75	3.76E-03	3.64
10	11.401	1	10	1.9	300	7.96	10.68	3.73E-03	3.61
10	11.401	1	10	1.9	360	7.97	10.65	3.71E-03	3.60
10	11.401	1	10	1.9	420	7.97	10.62	3.70E-03	3.59
Temp. 23° Average Steady State Measurement								3.71E-03	3.60
Single sample replicate precision at one standard deviation 1.29E-05 as a 0.00%						Precision estimated from error analysis ±10.2%			

Table C2. Site 1, hydraulic conductivity and permeability data for deformation zone; parallel to deformation bands (1.5cm) and parallel to bedding; sample D.

H [cm]	A [cm ²]	T [minute]	Chm-P [psi]	L [cm]	Elp-time [min.]	H-corret. [psi]	V [cm ³]	K [cm/s]	k [darcies]
30	11.401	1	10	2.4	0	28.97	4.24	5.13E-04	0.51
30	11.401	1	10	2.4	60	29.03	3.84	4.64E-04	0.46
30	11.401	1	10	2.4	120	29.18	2.92	3.51E-04	0.35
30	11.401	1	10	2.4	180	29.23	2.58	3.10E-04	0.31
30	11.401	1	10	2.4	240	29.29	2.20	2.64E-04	0.26
30	11.401	1	10	2.4	300	29.30	2.16	2.59E-04	0.26
30	11.401	1	10	2.4	360	29.30	2.14	2.56E-04	0.25
30	11.401	1	10	2.4	420	29.30	2.12	2.54E-04	0.25
Temp. 22° Average Steady State Measurement								2.56E-04	0.25
Single sample replicate precision at one standard deviation ±2.39E-07 or ±0.93%						Precision estimated from error analysis ±20.5%			

Table C3. Site 2, hydraulic conductivity and permeability data for deformation zone; parallel to deformation bands (0.4cm) and parallel to bedding; sample C.

H [cm]	A [cm ²]	T [minute]	Chm-P [psi]	L [cm]	Elp-time [min.]	H-corret. [psi]	V [cm ³]	K [cm/s]	k [darcies]
10	11.401	2	10	2.3	0	8.84	10.18	1.94E-03	1.88
10	11.401	2	10	2.3	60	8.92	9.14	1.72E-03	1.67
10	11.401	2	10	2.3	120	8.98	8.34	1.56E-03	1.51
10	11.401	2	10	2.3	180	9.07	7.21	1.34E-03	1.30
10	11.401	2	10	2.3	240	9.11	6.68	1.23E-03	1.20
10	11.401	2	10	2.3	300	9.11	6.65	1.23E-03	1.19
10	11.401	2	10	2.3	360	9.11	6.64	1.23E-03	1.19
10	11.401	2	10	2.3	420	9.11	6.62	1.22E-03	1.18
Temp. 23° Average Steady State Measurement								1.22E-03	1.19
Single sample replicate precision at one standard deviation ±2.82E-06 or ±0.23%						Precision estimated from error analysis ±11.1%			

Table C4. Site 2, hydraulic conductivity and permeability data for deformation zone parallel to deformation bands (0.2cm) and parallel to bedding; sample D.

H [cm]	A [cm ²]	T [minute]	Chm-P [psi]	L [cm]	Elp-time [min.]	H-corret. [psi]	V [cm ³]	K [cm/s]	k [darcies]
10	11.401	1	10	2.4	0	8.12	9.67	4.18E-03	3.96
10	11.401	1	10	2.4	60	8.26	8.79	3.73E-03	3.54
10	11.401	1	10	2.4	120	8.39	7.98	3.34E-03	3.16
10	11.401	1	10	2.4	180	8.48	7.37	3.05E-03	2.89
10	11.401	1	10	2.4	240	8.50	7.24	2.99E-03	2.83
10	11.401	1	10	2.4	300	8.50	7.22	2.98E-03	2.82
10	11.401	1	10	2.4	360	8.50	7.22	2.98E-03	2.82
10	11.401	1	10	2.4	420	8.51	7.20	2.97E-03	2.81
Temp. 24° Average Steady State Measurement								2.98E-03	2.82
Single sample replicate precision at one standard deviation ±6.78E-06 or ± 0.23%						Precision estimated from error analysis ±11.1%			

Table C5. Site 1, hydraulic conductivity and permeability data for deformation zone; perpendicular to deformation bands (0.2cm) and parallel to bedding; sample E.

H [cm]	A [cm ²]	T [minute]	Chm-P [psi]	L [cm]	Elp-time [min.]	H-corret. [psi]	V [cm ³]	K _{def.} [cm/s]	K _{avg} [cm/s]	k _{avg} [darcies]
45	11.401	5	10	2.3	0	44.41	7.00	9.32E-06	1.06E-04	0.11
45	11.401	5	10	2.3	60	44.43	6.34	8.43E-06	9.60E-05	0.10
45	11.401	5	10	2.3	120	44.45	5.83	7.74E-06	8.82E-05	0.09
45	11.401	5	10	2.3	180	44.48	4.75	6.29E-06	7.18E-05	0.07
45	11.401	5	10	2.3	240	44.50	4.12	5.45E-06	6.23E-05	0.06
45	11.401	5	10	2.3	300	44.52	3.76	4.97E-06	5.68E-05	0.06
45	11.401	5	10	2.3	360	44.53	3.26	4.30E-06	4.92E-05	0.05
45	11.401	5	10	2.3	420	44.54	3.02	3.98E-06	4.56E-05	0.05
45	11.401	5	10	2.3	480	44.55	2.64	3.48E-06	3.98E-05	0.04
45	11.401	5	10	2.3	540	44.55	2.58	3.40E-06	3.89E-05	0.04
45	11.401	5	10	2.3	600	44.55	2.55	3.36E-06	3.85E-05	0.04
Temp. 22° Average Steady State Measurement								3.41E-06	3.91E-05	0.04
Single sample replicate precision at one standard deviation ±6.92E-07 or ±1.77%						Precision estimated from error analysis ±18.0%				

Table C6. Site 1, hydraulic conductivity and permeability data for deformation zone; perpendicular to deformation bands (0.6cm) and parallel to bedding; sample F.

H [cm]	A [cm ²]	T [minute]	Chm-P [psi]	L [cm]	Elp-time [min.]	H-correct. [psi]	V [cm ³]	K _{def.} [cm/s]	K _{avg} [cm/s]	k _{avg} [darcies]
45	11.401	10	10	2.6	0	44.58	3.51	6.92E-06	2.99E-05	0.03
45	11.401	10	10	2.6	60	44.58	3.08	6.07E-06	2.63E-05	0.02
45	11.401	10	10	2.6	120	44.59	2.69	5.30E-06	2.29E-05	0.02
45	11.401	10	10	2.6	180	44.60	2.11	4.16E-06	1.80E-05	0.02
45	11.401	10	10	2.6	240	44.60	1.86	3.66E-06	1.59E-05	0.02
45	11.401	10	10	2.6	300	44.61	1.43	2.81E-06	1.22E-05	0.01
45	11.401	10	10	2.6	360	44.61	1.29	2.54E-06	1.10E-05	0.01
45	11.401	10	10	2.6	420	44.61	1.19	2.34E-06	1.01E-05	0.01
45	11.401	10	10	2.6	480	44.61	1.14	2.24E-06	9.71E-06	0.01
45	11.401	10	10	2.6	540	44.61	1.14	2.24E-06	9.71E-06	0.01
45	11.401	10	10	2.6	600	44.61	1.13	2.22E-06	9.63E-06	0.01
Temp. 24° Average Steady State Measurement								2.24E-06	9.68E-06	0.01
Single sample replicate precision at one standard deviation ±4.92E-08 or ±0.51%							Precision estimated from error analysis ±33.2%			

Table C7. Site 1, hydraulic conductivity and permeability data for deformation zone; perpendicular to deformation bands (1.4cm) and parallel to bedding; sample G.

P-head [psi]	P-head.correct.. [psi]	L [cm]	A [cm ²]	Chm-P [psi]	Flowrate [ml/min.]	Elp-time [min.]	K _{def.} [cm/s]	K _{avg} [cm/s]	k _{avg} [darcies]	
25	24.93	2.5	11.401	40	5.55	0	6.46E-06	1.15E-05	1.12E-02	
25	24.95	2.5	11.401	40	3.88	60	4.51E-06	8.05E-06	7.81E-03	
25	24.95	2.5	11.401	40	3.21	120	3.74E-06	6.67E-06	6.47E-03	
25	24.96	2.5	11.401	40	2.88	180	3.35E-06	5.98E-06	5.80E-03	
25	24.96	2.5	11.401	40	2.57	240	2.99E-06	5.33E-06	5.17E-03	
25	24.97	2.5	11.401	40	2.21	300	2.57E-06	4.59E-06	4.45E-03	
25	24.97	2.5	11.401	40	2.00	360	2.33E-06	4.16E-06	4.03E-03	
25	24.97	2.5	11.401	40	1.99	420	2.31E-06	4.12E-06	4.00E-03	
25	24.97	2.5	11.401	40	1.96	480	2.27E-06	4.06E-06	3.94E-03	
25	24.97	2.5	11.401	40	1.95	540	2.27E-06	4.05E-06	3.92E-03	
25	24.97	2.5	11.401	40	1.95	600	2.26E-06	4.04E-06	3.92E-03	
Temp. 23° Average Steady State Measurement							2.27E-06	4.05E-06	3.93E-03	
Single sample replicate precision at one standard deviation ±8.64E-09 or ±0.21%							Precision estimated from error analysis ±6.7%			

Table C8. Site 1, hydraulic conductivity and permeability data for deformation zone; perpendicular to deformation bands (1.5cm) and parallel to bedding; sample H.

P-head [psi]	P-head.corret.. [psi]	L [cm]	A [cm ²]	Chm-P [psi]	Flowrate [ml/min.]	Elp-time [min.]	K _{def.} [cm/s]	K _{avg} [cm/s]	k _{avg} [darcies]
25	24.92	2.2	11.401	40	6.44	0	8.03E-06	1.18E-05	1.14E-02
25	24.93	2.2	11.401	40	5.66	60	7.06E-06	1.04E-05	1.00E-02
25	24.94	2.2	11.401	40	4.34	120	5.42E-06	7.94E-06	7.70E-03
25	24.95	2.2	11.401	40	3.43	180	4.28E-06	6.27E-06	6.08E-03
25	24.96	2.2	11.401	40	2.97	240	3.70E-06	5.42E-06	5.26E-03
25	24.96	2.2	11.401	40	2.76	300	3.44E-06	5.05E-06	4.90E-03
25	24.96	2.2	11.401	40	2.46	360	3.06E-06	4.49E-06	4.36E-03
25	24.96	2.2	11.401	40	2.33	420	2.91E-06	4.26E-06	4.14E-03
25	24.97	2.2	11.401	40	2.13	480	2.65E-06	3.89E-06	3.77E-03
25	24.97	2.2	11.401	40	2.12	540	2.64E-06	3.88E-06	3.76E-03
25	24.97	2.2	11.401	40	2.12	600	2.64E-06	3.87E-06	3.75E-03
Temp. 23° Average Steady State Measurement							2.65E-06	3.88E-06	3.76E-03
Single sample replicate precision at one standard deviation ±1.12E-08 or ±0.29%						Precision estimated from error analysis ±7.0%			

Table C9. Site 2, hydraulic conductivity and permeability data for deformation zone; perpendicular to deformation bands (0.1cm) and parallel to bedding; sample E.

H [cm]	A [cm ²]	T [minute]	Chm-P [psi]	L [cm]	Elp-time [min.]	H-corret. [psi]	V [cm ³]	K _{def.} [cm/s]	K _{avg} [cm/s]	k _{avg} [darcies]
30	11.401	5	10	2.1	0	28.34	41.29	5.69E-05	8.95E-04	0.87
30	11.401	5	10	2.1	60	28.47	37.24	4.94E-05	8.03E-04	0.78
30	11.401	5	10	2.1	120	28.63	32.20	4.08E-05	6.91E-04	0.67
30	11.401	5	10	2.1	180	28.77	27.77	3.39E-05	5.93E-04	0.57
30	11.401	5	10	2.1	240	28.87	24.49	2.91E-05	5.21E-04	0.51
30	11.401	5	10	2.1	300	28.93	22.42	2.62E-05	4.76E-04	0.46
30	11.401	5	10	2.1	360	29.00	20.20	2.31E-05	4.28E-04	0.41
30	11.401	5	10	2.1	420	29.04	19.13	2.17E-05	4.04E-04	0.39
30	11.401	5	10	2.1	480	29.04	19.08	2.17E-05	4.03E-04	0.39
30	11.401	5	10	2.1	540	29.04	19.07	2.17E-05	4.03E-04	0.39
30	11.401	5	10	2.1	600	29.04	19.07	2.17E-05	4.03E-04	0.39
Temp. 23° Average Steady State Measurement								2.17E-05	4.03E-04	0.39
Single sample replicate precision at one standard deviation ±1.22E-07 or ±0.03%						Precision estimated from error analysis ±7.8%				

Table C10. Site 2, hydraulic conductivity and permeability data for deformation zone; perpendicular to deformation bands (0.3cm) and parallel to bedding; sample F.

H [cm]	A [cm ²]	T [minute]	Chm-P [psi]	L [cm]	Elp-time [min.]	H-correct. [psi]	V [cm ³]	K _{def.} [cm/s]	K _{avg} [cm/s]	k _{avg} [darcies]
45	11.401	10	10	2.2	0	44.49	9.12	9.14E-06	6.59E-05	0.07
45	11.401	10	10	2.2	60	44.51	7.78	7.78E-06	5.62E-05	0.06
45	11.401	10	10	2.2	120	44.53	6.62	6.60E-06	4.78E-05	0.05
45	11.401	10	10	2.2	180	44.54	5.74	5.71E-06	4.14E-05	0.04
45	11.401	10	10	2.2	240	44.57	3.92	3.89E-06	2.83E-05	0.03
45	11.401	10	10	2.2	300	44.59	3.01	2.98E-06	2.17E-05	0.02
45	11.401	10	10	2.2	360	44.59	2.72	2.69E-06	1.96E-05	0.02
45	11.401	10	10	2.2	420	44.59	2.55	2.52E-06	1.84E-05	0.02
45	11.401	10	10	2.2	480	44.60	2.25	2.22E-06	1.62E-05	0.02
45	11.401	10	10	2.2	540	44.60	2.24	2.21E-06	1.62E-05	0.02
45	11.401	10	10	2.2	600	44.60	2.22	2.19E-06	1.60E-05	0.02
Temp. 22° Average Steady State Measurement								2.21E-06	1.61E-05	0.02
Single sample replicate precision at one standard deviation ±1.10E-07 or ±0.68%							Precision estimated from error analysis ±20.2%			

Table C11. Site 2, hydraulic conductivity and permeability data for deformation zone; perpendicular to deformation bands (0.2cm) and parallel to bedding; sample G.

P-head [psi]	P-head.correct.. [psi]	L [cm]	A [cm ²]	Chm-P [psi]	Flowrate [ml/min.]	Elp-time [min.]	K _{def.} [cm/s]	K _{avg} [cm/s]	k _{avg} [darcies]
10	9.52	1.9	11.401	20	84.46	0	4.05E-05	3.49E-04	0.35
10	9.58	1.9	11.401	20	70.57	60	3.31E-05	2.90E-04	0.29
10	9.60	1.9	11.401	20	64.21	120	2.98E-05	2.63E-04	0.26
10	9.63	1.9	11.401	20	57.42	180	2.64E-05	2.35E-04	0.23
10	9.67	1.9	11.401	20	49.41	240	2.24E-05	2.01E-04	0.20
10	9.70	1.9	11.401	20	43.24	300	1.94E-05	1.76E-04	0.17
10	9.75	1.9	11.401	20	32.56	360	1.43E-05	1.32E-04	0.13
10	9.78	1.9	11.401	20	27.47	420	1.20E-05	1.11E-04	0.11
10	9.79	1.9	11.401	20	25.24	480	1.10E-05	1.02E-04	0.10
10	9.79	1.9	11.401	20	24.37	540	1.06E-05	9.80E-05	0.10
10	9.80	1.9	11.401	20	24.31	600	1.06E-05	9.77E-05	0.10
Temp. 22° Average Steady State Measurement							1.07E-05	9.91E-05	0.10
Single sample replicate precision at one standard deviation ±2.13E-06 or ±2.15%						Precision estimated from error analysis ±10.0%			

Table C12. Site 2, hydraulic conductivity and permeability data for deformation zone; perpendicular to deformation bands (0.5cm) and parallel to bedding; sample H.

P-head [psi]	P-head.corret.. [psi]	L [cm]	A [cm ²]	Chm-P [psi]	Flowrate [ml/min.]	Elp-time [min.]	K _{def.} [cm/s]	K _{avg} [cm/s]	k _{avg} [darcies]
10	9.84	2.3	11.401	20	17.67	0	1.90E-05	8.56E-05	0.08
10	9.85	2.3	11.401	20	16.25	60	1.74E-05	7.86E-05	0.07
10	9.85	2.3	11.401	20	15.69	120	1.68E-05	7.59E-05	0.07
10	9.86	2.3	11.401	20	13.88	180	1.48E-05	6.71E-05	0.06
10	9.88	2.3	11.401	20	12.04	240	1.28E-05	5.81E-05	0.06
10	9.89	2.3	11.401	20	10.37	300	1.10E-05	5.00E-05	0.05
10	9.91	2.3	11.401	20	8.11	360	8.56E-06	3.90E-05	0.04
10	9.91	2.3	11.401	20	7.26	420	7.65E-06	3.49E-05	0.03
10	9.92	2.3	11.401	20	7.13	480	7.51E-06	3.43E-05	0.03
10	9.92	2.3	11.401	20	7.13	540	7.51E-06	3.43E-05	0.03
10	9.92	2.3	11.401	20	7.10	600	7.48E-06	3.41E-05	0.03
Temp. 24° Average Steady State Measurement							7.50E-06	3.42E-05	0.03
Single sample replicate precision at one standard deviation ±8.32E-08 or ±0.24%						Precision estimated from error analysis ±9.8%			

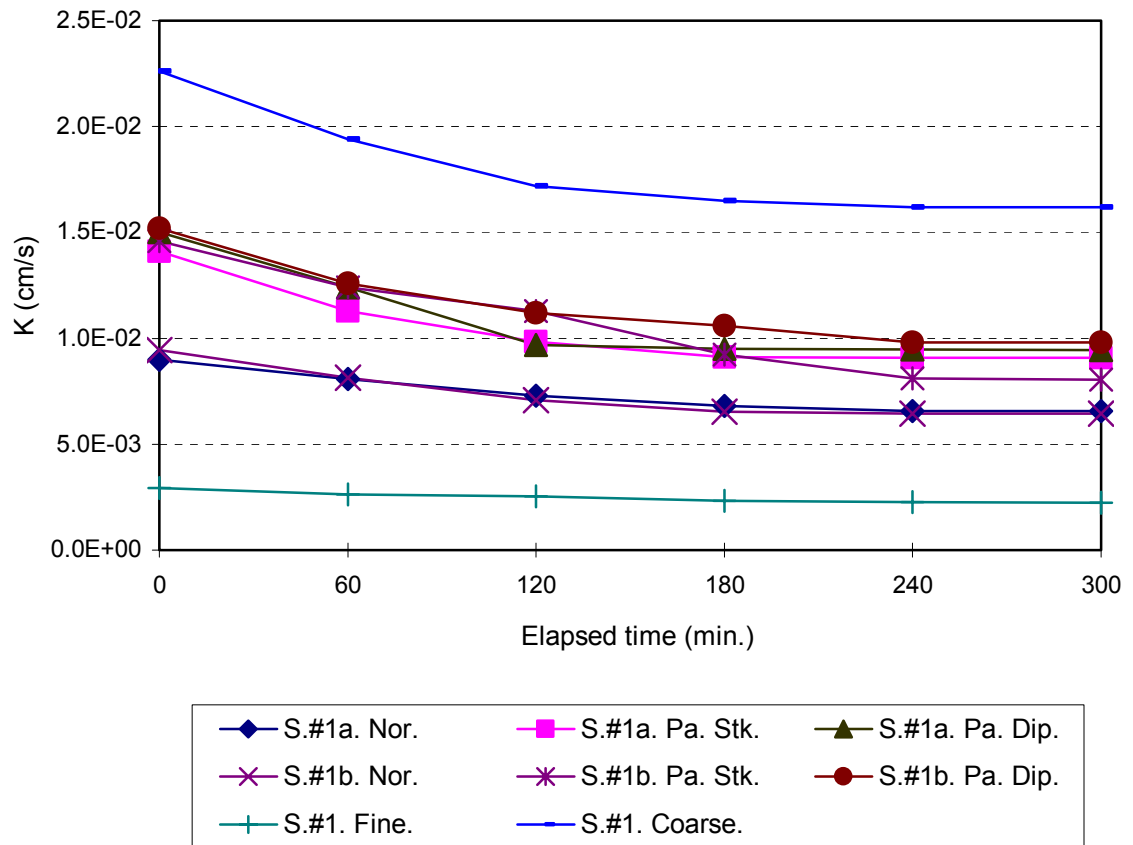


Figure A1. Hydraulic conductivity of undeformed sands, Site 1.

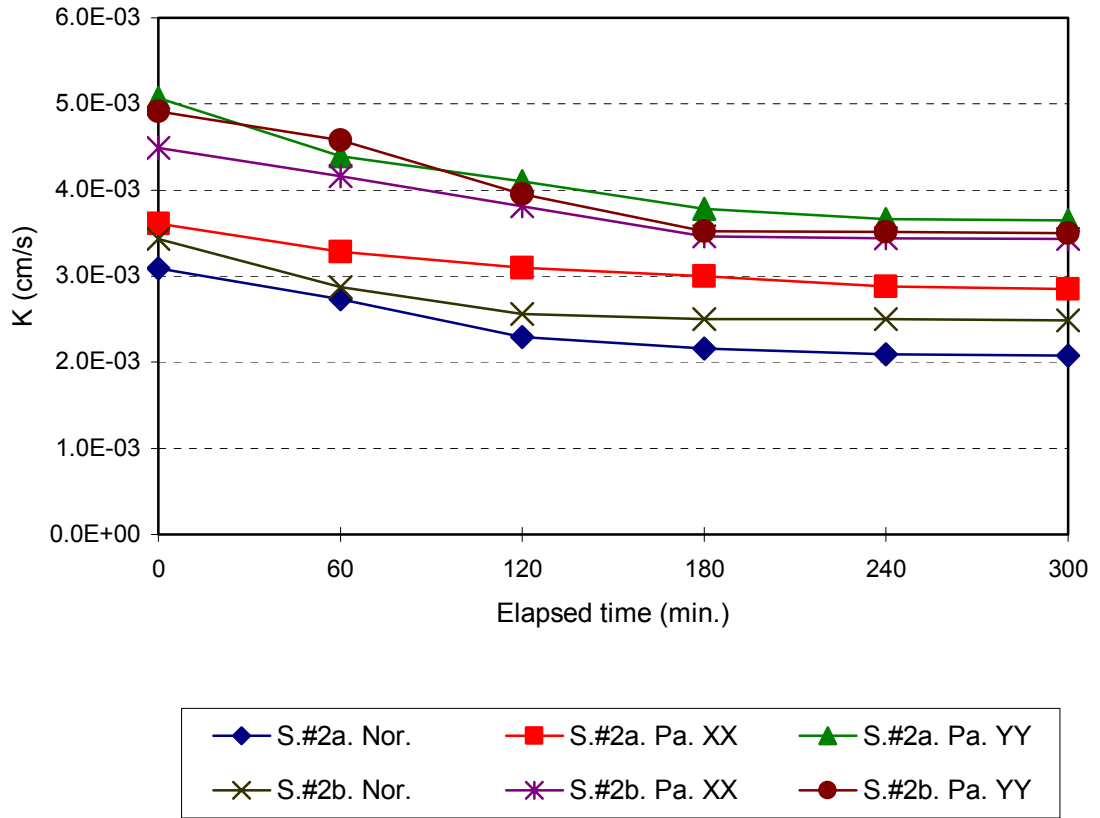


Figure A2. Hydraulic conductivity of undeformed sands, Site 2.

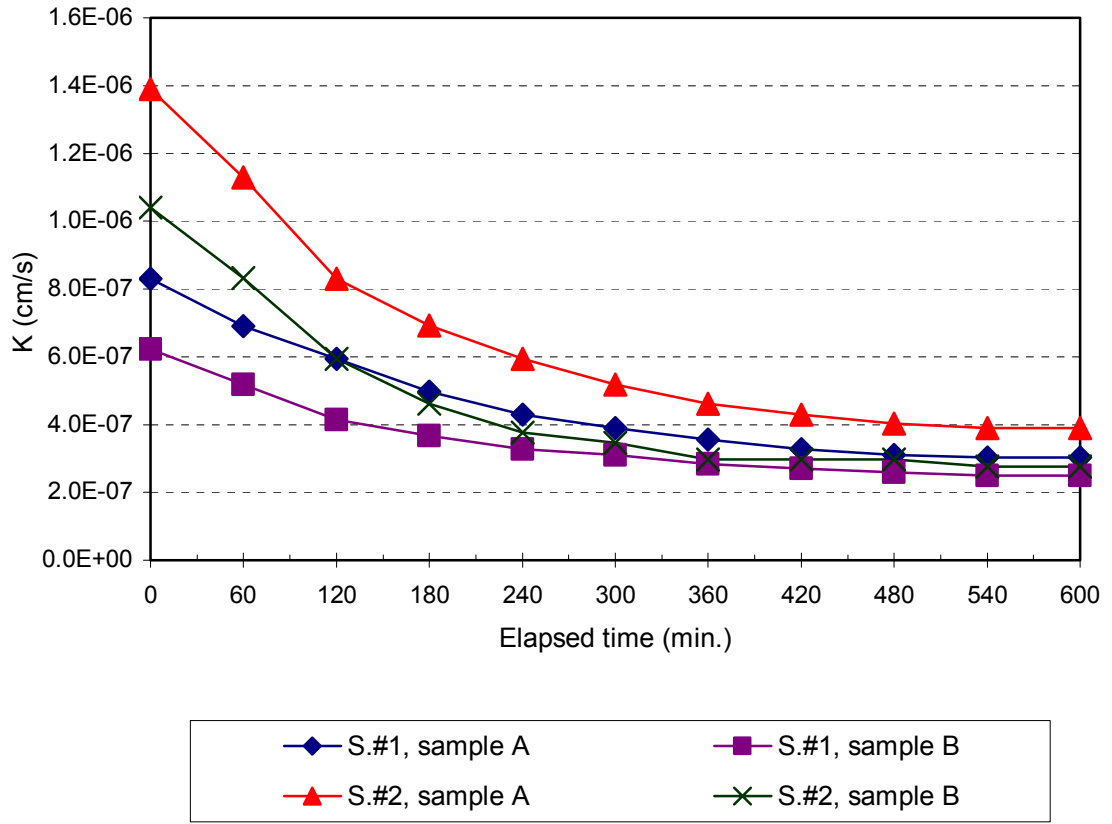


Figure A3. Hydraulic conductivity of perpendicular to deformation bands; homogeneous sample, Site 1 and 2.

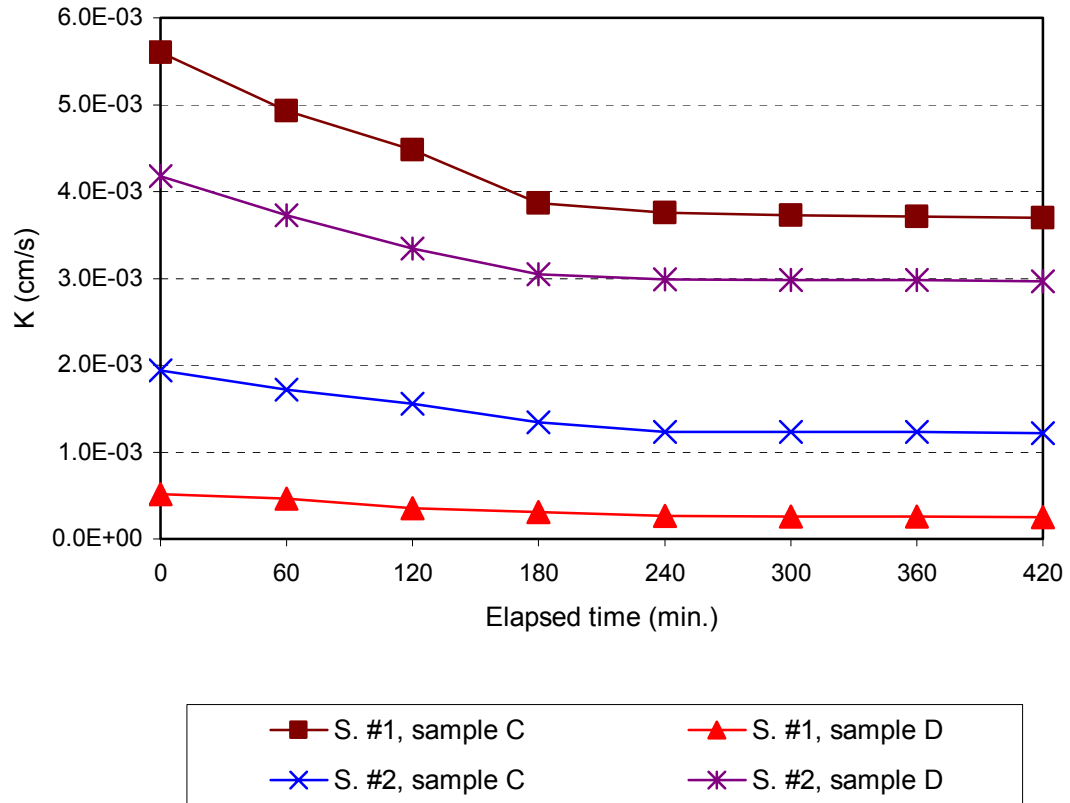


Figure A4. Hydraulic conductivity of deformation zone; parallel to deformation bands in composite sample, Site 1 and 2.

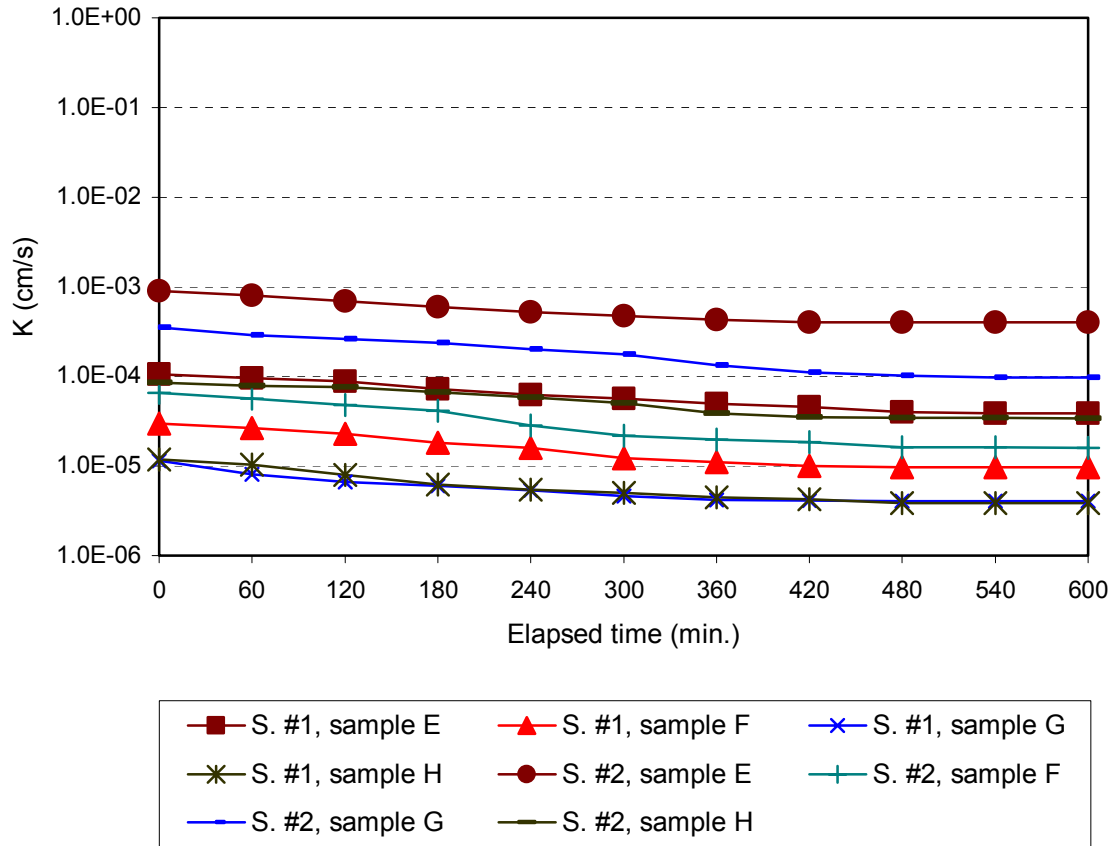


Figure A5. Hydraulic conductivity of deformation zone; perpendicular to deformation bands in composite sample, Site 1 and 2.

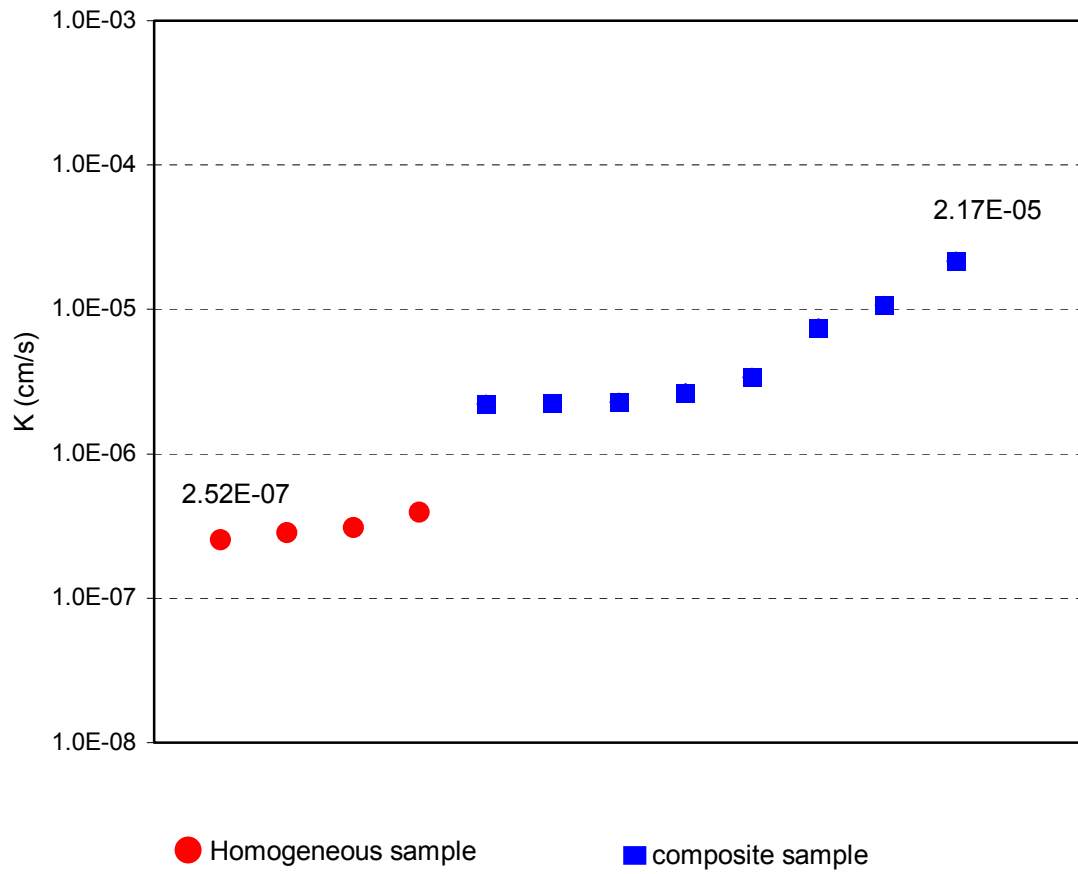


Figure A6. Variation of hydraulic conductivity of perpendicular to deformation bands; end member's value of K is shown in the graph.